Chapter 9

Epitaxy and Device Properties of InGaAs Photodetectors with Relatively High Lattice Mismatch

Xing-you Chen, Yi Gu and Yong-gang Zhang

Additional information is available at the end of the chapter

http://dx.doi.org/10.5772/intechopen.70259

Abstract

In this chapter, our works on the developments of wavelength-extended InGaAs photodetectors with cutoff wavelength >1.7 μm are reviewed. Various InGaAs/InAlAs p-i-n heterojunction structures have been grown on InP and GaAs substrates by gas source molecular beam epitaxy, some details on the InGaAs photodetector structures and the techniques of metamorphic buffer layer such as linearly, step, and one-step continuously InAlAs graded buffer, and dislocation restraint methods of compositional overshoot and digital alloy are introduced. The material characteristics and device properties were evaluated by atomic force microscopy, high-resolution X-ray diffraction and reciprocal space mapping, cross-sectional transmission electron microscopy, and current-voltage measurements, etc. The results provide clues to the development of metamorphic device structures on lattice-mismatched material systems.

Keywords: InGaAs, photodetector, metamorphic, lattice mismatch, X-ray diffraction, atomic force microscopy, photoluminescence

1. Introduction

InGaAs photodetectors (PDs) and focal plane arrays (FPAs) are attracting particular interests as they can be tailored to cover one of the atmospheric windows of 1–3 μm in short-wave infrared band. The $In_{0.53}Ga_{0.47}As$ PDs grown lattice-matched to InP are commercially mature with cutoff wavelength at 1.7 μm. Wavelength-extended $In_xGa_{1-x}As$/InP ($0.53 < x < 1$) PDs with cutoff wavelength more than 1.7 μm have been extensively investigated over the past decades due to their important applications in spatial remote sensing, earth observation, environmental monitoring, etc. [1, 2]. However, for application in longer wavelength region, the indium content should be increased, which increases the lattice mismatch

between high indium content InGaAs and InP substrate. For instance, the $In_{0.83}Ga_{0.17}As$ PD with cutoff wavelength of 2.5 μm possesses a lattice mismatch of about +2.1% with respect to InP. In that case, the dark current increases several orders of magnitude, which severely hinders the development of wavelength-extended InGaAs PDs in the infrared range. To suppress the dark current of InGaAs PD, it is a prerequisite to optimize the InGaAs material with high indium (In) content. Therefore, high In content $In_xGa_{1-x}As$ has been grown on InP, GaAs, and Si substrate by using techniques such as molecular beam epitaxy (MBE) and metal organic chemical vapor deposition (MOCVD). During the process of material growth, dislocation restriction techniques such as beryllium (Be) doping [3], dilute nitride [4], strained or strain-compensated superlattice (SL), and strain-driven quantum dots (QDs) were adopted to reduce the threading dislocation density (TDD) in the metamorphic buffer layer (MBL). Several sets of results with different x values of the $In_xGa_{1-x}As$ layers are listed in **Table 1**. Our own results are also included. It can be seen that the TDD could be quite different for InGaAs with various In contents due to different lattice mismatches with different substrates.

In this chapter, the InGaAs/InAlAs p-i-n heterojunction structure was always used for the growth of wavelength-extended InGaAs PD with high indium content because of higher quantum efficiency than homostructure. Both the MBL schemes and experimental parameters have

X value	Growth method	Substrate	TDD in $In_xGa_{1-x}As$ (cm^{-2})	Reference
0.68	MOCVD	InP (0 0 1)	~10^6 (XTEM)	Ji et al. [5]
0.82	MOCVD	InP (0 0 1)	~10^8 (XTEM)	Zhao et al. [6]
0.82	MOCVD	InP (0 0 1)	~10^{11}–10^{12} (XRD-FWHM)	Zhao et al. [7]
0.83	GSMBE	InP (0 0 1)	≤10^7 (XTEM)	Present work
0.53	SSMBE	GaAs (0 0 1)	~10^6 (XTEM)	Lubyshev et al. [8]
0.6	SSMBE	GaAs (0 0 1)	~10^8 (XTEM)	Valtuefia et al. [9]
0.75–1	SSMBE	GaAs (0 0 1)	~10^9–10^{10} (plan-view TEM)	Chang et al. [10]
1	SSMBE	GaAs (0 0 1)	~10^8–10^9 (XTEM)	Chang et al. [11]
0.8	Not mentioned	GaAs (0 0 1)	~10^5 (EPD)	Zimmermann et al. [12]
0.63	SSMBE	GaAs (0 0 1)	~10^8 (XTEM)	Song et al. [13]
0.85	SSMBE	GaAs (0 0 1)	Not mentioned	Jurczak et al. [14]
0.83	GSMBE	GaAs (0 0 1)	~10^9–10^{10} (XTEM)	Present work
0.53	SSMBE	Si (1 1 1)	Not mentioned	Gao et al. [15]

Table 1. Parameters of $In_xGa_{1-x}As$ ($0.53 \leq x \leq 1$) as reported by various researchers.

been optimized to acquire high-performance InGaAs PDs with relatively high-lattice mismatch. Additionally, some strategies were used to reduce the residual strain and decrease the TDD, such as composition overshoot and the insertion of digital alloy (DA) intermediate layer in the MBL.

All the material growth in this chapter was performed in a VG Semicon V80H gas source molecular beam epitaxy (GSMBE) system. The best background chamber pressure achieved in this system was about 3×10^{-11} Torr, and the pressure during growth is typically in the 10^{-5} Torr range. The elemental In, gallium (Ga), and aluminum (Al) sources were used as group III sources, and the elemental silicon (Si) and Be were used as n-type and p-type dopant sources, respectively. Their fluxes were controlled by changing the cell temperatures. Arsine and phosphine cracking cells were used as group V sources, and their fluxes were controlled by adjusting the pressure. The cracking temperature was approximately 1000°C measured by using a thermocouple. The growth rates were all adjusted to about 1 μm/h for InP, InAlAs, and InGaAs.

2. Optimize the growth of wavelength extended InGaAs PDs on InP

2.1. The effects of growth temperature on the characteristics of InP-based $In_{0.83}Ga_{0.17}As$ PDs

The growth temperature (T_g) is one of the most important parameters of MBE. To acquire high-device performance wavelength-extended InGaAs PD on InP substrate, the growth temperature should be optimized for each layer. Generally, a high T_g can reduce the incorporation of background impurities into the epilayers during the growth process, whereas the higher T_g will enhance the In segregation on the surface of InGaAs with a high In content [16], which will cause a poor surface and nonuniformity of compositions in the epilayer and then increase the dark current of PDs. In this work, T_g was optimized for the InAlAs buffer layer and InGaAs absorption layer, respectively [17].

Four $In_{0.83}Ga_{0.17}As$ PD structures with continuously graded InAlAs buffers were grown on (1 0 0)-oriented Fe-doped InP epi-ready substrate. Each structure consisted of a 1.95-μm N^+ ($N = 3 \times 10^{18}$ cm^{-3}) InAlAs buffer layer and a 2-μm-thick n^- ($n = 3 \times 10^{16}$ cm^{-3}) $In_{0.84}Ga_{0.16}As$ absorption layer followed by a P^+ ($P = 7 \times 10^{18}$ cm^{-3}) 600-nm-thick $In_{0.84}Al_{0.16}As$ cap. The In profiles and T_g at stages A, B, C, and D of the four PD structures were shown in **Figure 1**.

The results show that the growth temperature of the absorption layer should not be very low, whereas the InAlAs MBL with the T_g graded from 500 to 460°C exhibits better crystalline quality than that grown at either 460 or 500°C. The sample number 3 with InAlAs MBL grown with temperature graded from 500 to 460°C, and InGaAs absorption layer grown at 500°C exhibits better crystalline quality. It shows smoother surface with lower root-mean-square (RMS) of atomic force microscopy (AFM), narrower full width at half maximum (FWHM) of X-ray diffraction (XRD), and stronger photoluminescence (PL) intensity than others, as shown in **Figure 2**. Therefore, this temperature strategy for growth of wavelength-extended InGaAs PDs on InP substrate will be always used hereafter except for special reminding.

Sample no.	Growth temperature (˚C)			
	A	B	C	D
1	500	500	500	500
2	460	460	500	500
3	500	460	500	500
4	500	460	460	460

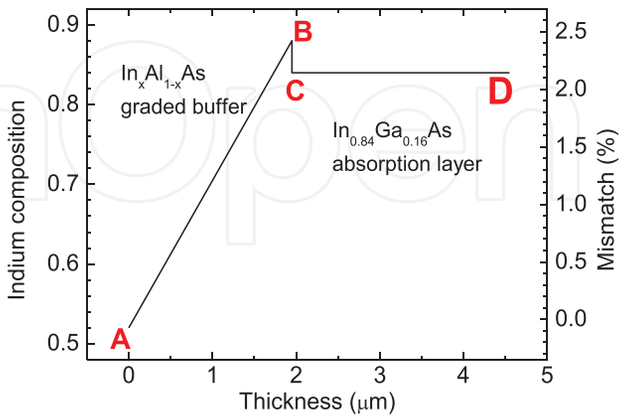

Figure 1. Growth temperatures at points A–D of the $In_{0.84}Ga_{0.16}As$ PD structures. The inset shows the indium composition vs. the grown thickness of samples 1–4. Reprinted with permission from Elsevier.

2.2. The optimization and comparison of PD structures on different metamorphic buffer layers

To acquire high-quality wavelength-extended InGaAs materials with relatively high-lattice mismatch, an appropriate InAlAs MBL is needed. Generally, for the growth of lattice-mismatched material system, the MBLs should be thick enough so that the lattice parameter can finally relax to be a freestanding status, and the misfit dislocation can annihilate ultimately during the growth process of the MBL. However, it is impractical and high cost to grow an excessively thick MBL for device structure by MBE technique due to a limited growth rate of around 1 μm h^{-1}. Therefore, proper schemes of thin MBL should be explored.

In our previous work, the effect of various kinds of MBL schemes such as a thick uniform buffer, continuously graded buffer, and step-graded buffer on the structural characteristics and device performances of InP-based InGaAs PDs has been compared [18–20].

Two $In_{0.83}Ga_{0.17}As$ PD wafers with continuously (sample S1) and step-graded (sample S2) InAlAs MBLs were grown on semi-insulated (S.I.) (1 0 0)-oriented InP epi-ready substrate. Each wafer consisted of a 1.9-μm N^+ ($N = 3 \times 10^{18}$ cm^{-3}) InAlAs MBL and a 1.5-μm-thick n^- ($n = 3 \times 10^{16}$ cm^{-3}) $In_{0.83}Ga_{0.17}As$ absorption layer followed by a P^+ ($P = 7 \times 10^{18}$ cm^{-3}) 530-nm-thick InAlAs cap layer. The typical schematic structures of the two PDs were shown in **Figure 3**.

The growth of sample S1 with a continuously graded $In_xAl_{1-x}As$ MBL started with a 200-nm InP buffer layer grown at 460°C, following a 0.1-μm-thick N^+ $In_{0.52}Al_{0.48}As$ layer grown at 500°C, the N^+ continuously graded $In_xAl_{1-x}As$ buffer layer was grown with growth temperature decreased linearly from 500 to 460°C, and the In composition x was graded from 0.52

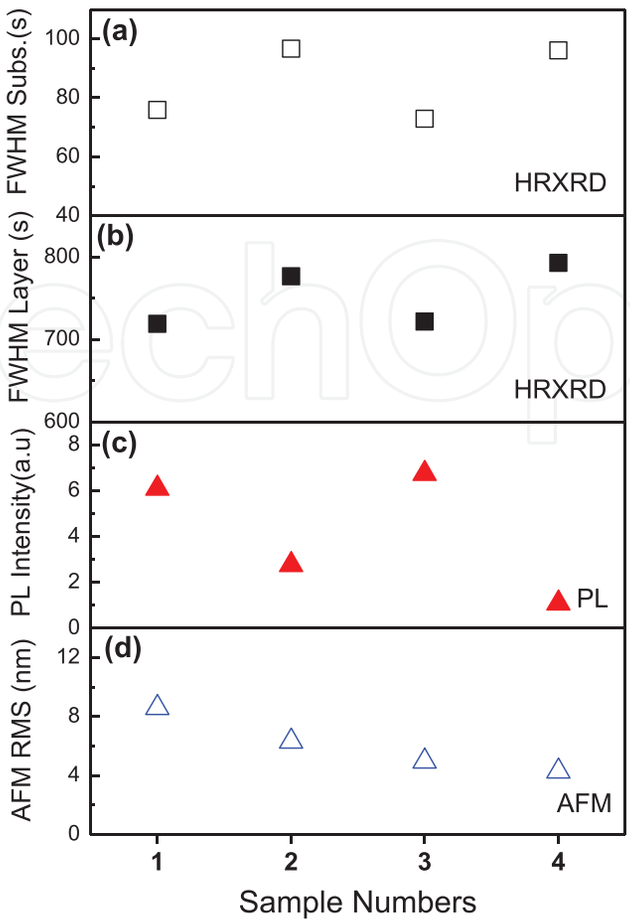

Figure 2. Summary of the measured data of samples with different temperature strategies. (a) HRXRD FWHM of substrate peak, (b) HRXRD FWHM of layer peak, (c) PL intensity of InGaAs absorption layer and (d) AFM RMS of samples 1–4. Reprinted with permission from Elsevier.

to 0.83 through the simultaneously linear increase of In source temperature and decrease of Al source temperature in a relatively small temperature region. This caused the In and Al beam fluxes to change with cell temperatures exponentially in opposite directions so that the composition grading profile in the buffer approximates a linear grade. The thickness of the InAlAs MBL was about 1.9 μm. After that, the growth temperature was increased to 490°C for the following growth.

The growth of sample S2 with a step-graded $In_xAl_{1-x}As$ MBL started with a 200-nm InP buffer layer grown at 460°C, following a 0.1-μm-thick N^+ $In_{0.52}Al_{0.48}As$ layer grown at 500°C, and then four N^+ $In_xAl_{1-x}As$ buffer layers with In composition of 0.60, 0.68, 0.76, and 0.83 were grown in sequence at 490, 480, 470, and 460°C, respectively. The In composition x was step graded from 0.52 to 0.83. Therefore, the thickness of the step-graded InAlAs MBL was also about 1.9 μm with each step layer of about 475 nm. After that, the growth temperature was kept at 490°C for the following growth.

To reduce the conduction band discontinuity and the dislocation density between the InGaAs absorption layer and InAlAs buffer and cap layers due to the small lattice mismatch between

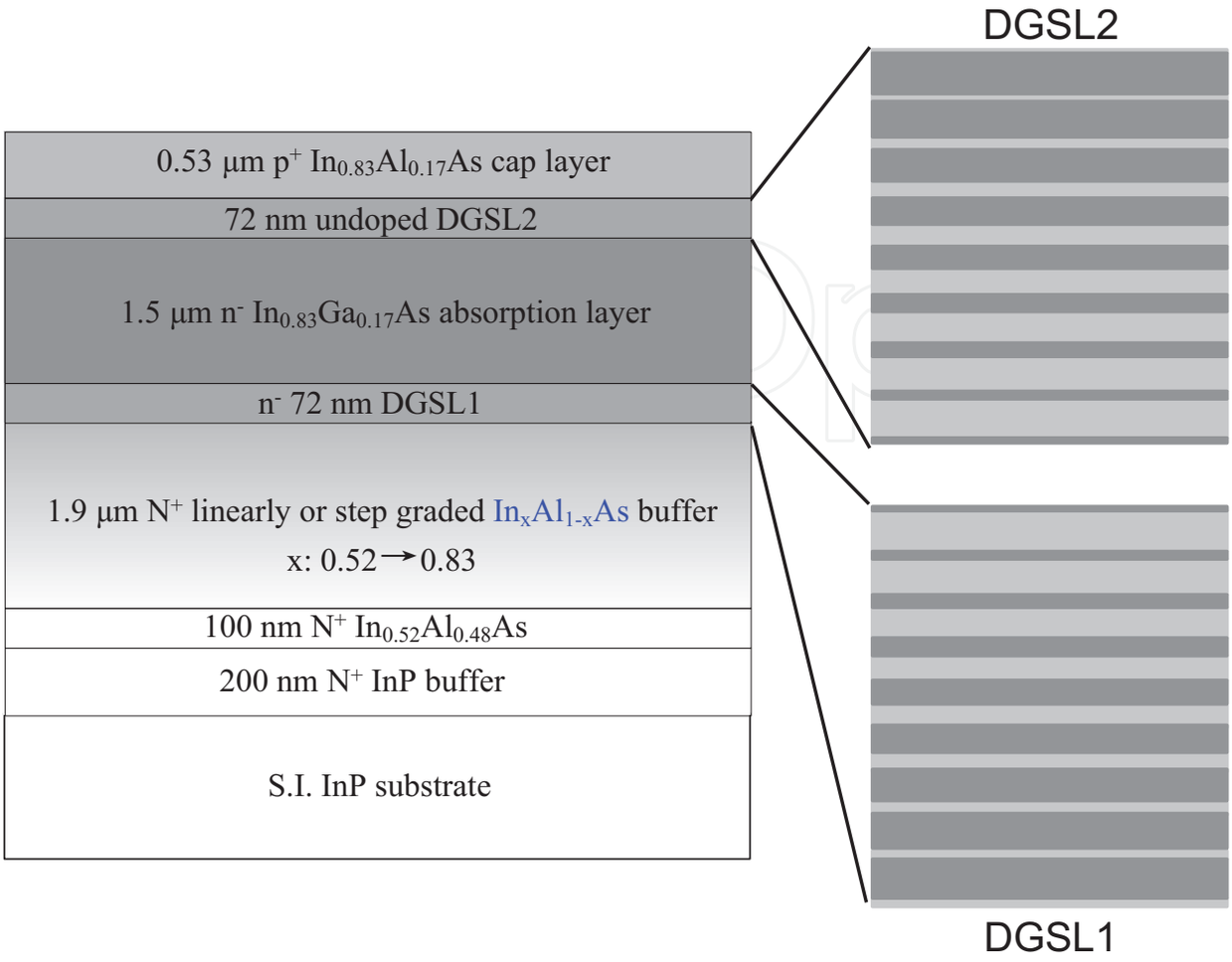

Figure 3. The schematic structure of $In_{0.83}Ga_{0.17}As$ photodetectors.

InGaAs and InAlAs at the interfaces, digital-graded superlattices (DGSLs) were grown at the interfaces, respectively. First, DGSL1 consisted of nine groups of $In_{0.83}Ga_{0.17}As/In_{0.83}Al_{0.17}As$ thin films which alternate with each other. The thickness of each group is about 8 nm. The thickness ratios of $In_{0.83}Ga_{0.17}As/In_{0.83}Al_{0.17}As$ in each group are 1:9, 2:8, …, finally coming to …, 8:2, 9:1, respectively. Similarly, DGSL2 was comprised of nine groups of $In_{0.83}Al_{0.17}As/In_{0.83}Ga_{0.17}As$ thin films which also alternate with each other but in a reverse order, and the thickness ratios of $In_{0.83}Al_{0.17}As/In_{0.83}Ga_{0.17}As$ in each group are 1:9, 2:8, …, finally coming to …, 8:2, 9:1, respectively. It is similar to the chirped $In_{0.53}Ga_{0.47}As/In_{0.52}Al_{0.48}As$ superlattice-graded bandgap layer used in some literatures [21–23].

Figure 4(a) shows the two different growth profiles of the In composition of $In_xAl_{1-x}As$ buffer for the InP-based $In_{0.83}Ga_{0.17}As$ PDs. Through a comprehensive comparison, sample S1 with continuously graded $In_xAl_{1-x}As$ MBL shows better properties on both material and devices than that of sample S2 with step-graded $In_xAl_{1-x}As$ MBL. As shown in the cross-sectional transmission electron micrographs (XTEMs) of **Figure 5**, almost none evident TD was found in the absorption layer of sample S1. By contrast, some obvious TDs exist in the absorption layer of sample S2. Unsurprisingly, sample S1 shows superior device performance compared

http://dx.doi.org/10.5772/intechopen.70259

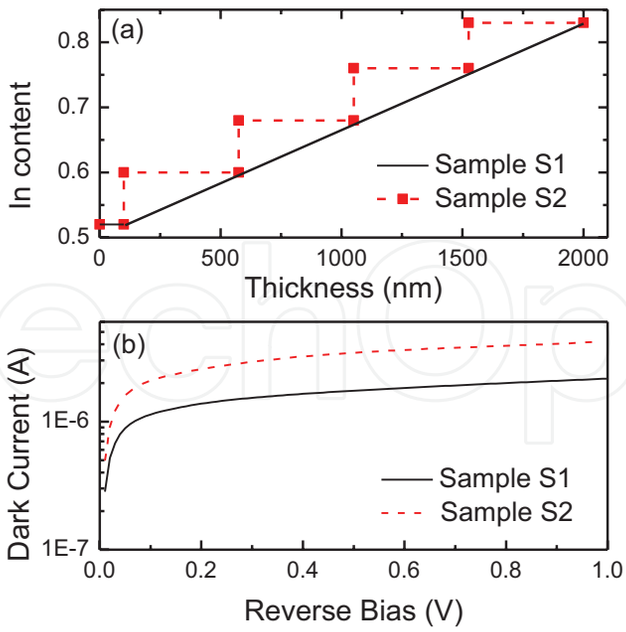

Figure 4. (a) The profiles of the indium composition vs. the grown thickness, and (b) I-V characteristics at 300 K of samples S1 and S2.

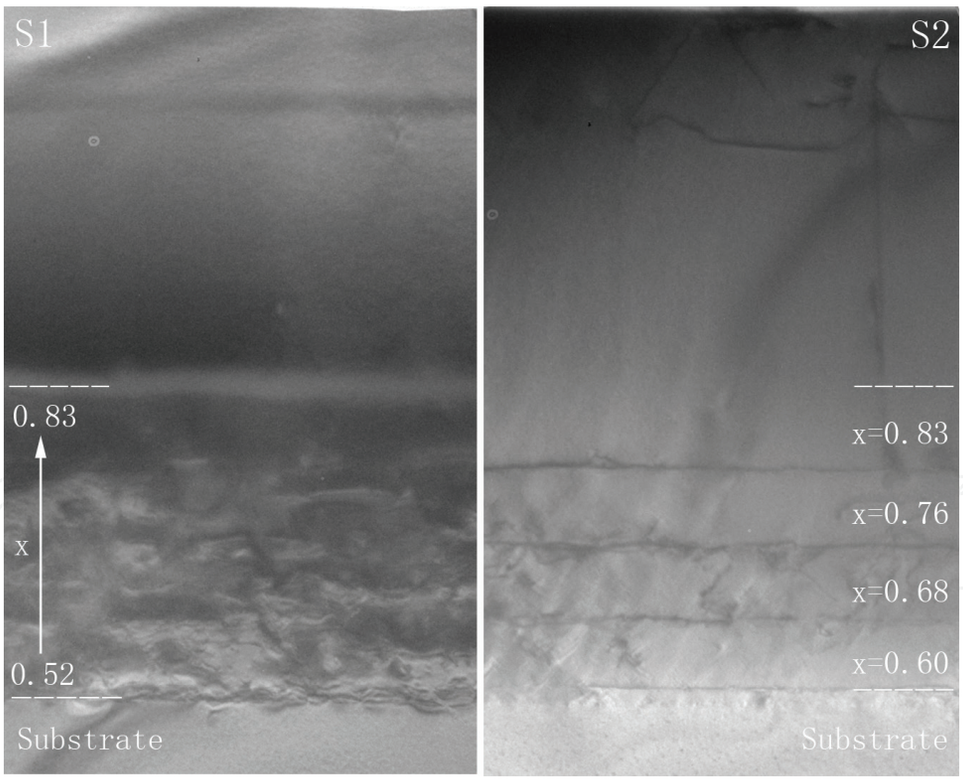

Figure 5. XTEM images of samples S1 and S2.

to sample S2. By measuring the mesa-type devices in diameter size of 200 μm, the room temperature (RT) dark current of the sample S1 was smaller than that of sample S2 at low reverse bias condition, as shown in **Figure 4(b)**. At reverse bias of −10 mV, the dark currents are 259 nA

(8.25×10^{-4} A/cm^2) and 473 nA (1.51×10^{-3} A/cm^2) for samples S1 and S2, respectively. Therefore, continuously graded $In_xAl_{1-x}As$ MBL scheme is more suitable for the growth of $In_{0.83}Ga_{0.17}As$ PDs on InP substrate.

In the previous continuously graded InAlAs MBLs, all the In contents were graded from 0.52. The initial lattice constant matches to the InP substrate. Strain energies in the continuously graded buffer increase gradually with increasing In content. Then, dispersed misfit dislocations will be generated to release the strain energy slowly in the buffer. Little overlap and interaction would occur among the TDs. Thus, an enough thick buffer is needed to slide and annihilate the TDs during the growth process. Here, we propose another method to promote the overlap of dispersed TDs by introducing an abrupt initial $In_yAl_{1-y}As$ ($y > 0.52$) layer of InAlAs MBL on InP substrate. This abrupt initial layer, mismatched with the InP substrate, is similar to a step buffer. But it was combined with a continuously graded $In_xAl_{1-x}As$ buffer with x graded from y to the composition needed. This buffer scheme, so-called one-step continuously graded buffer, is expected to possess the advantages of both step and continuously graded schemes. The strain is released rapidly by introducing the initial abrupt buffer, and TDs were restricted between the step buffer and the InP substrate. We show that this method results in lower TDD in the final-graded buffer and the InGaAs absorption layer in the wavelength-extended PD structure. This buffer strategy has been also adopted and demonstrated for the growth of $InAs_xP_{1-x}$ on InP by MOCVD method [23].

To investigate the effect of this buffer scheme on the properties of InP-based $In_{0.83}Ga_{0.17}As$ PDs with a lattice mismatch of 2.1%. Samples with three different initial In compositions were grown by GSMBE. As a comparison, the In composition grading profile and growth method of sample E were remained the same as before [19, 24]. For the deposition of wafers with one-step continuously graded $In_yAl_{1-y}As$ buffer, the In contents y of the one-step buffer were set to be 0.68 and 0.77 with the thicknesses of 0.5 and 0.7 μm, respectively. Then, the one-step buffer was followed by a continuously graded $In_xAl_{1-x}As$ buffer with In composition graded from 0.68 or 0.77 to 0.83, respectively. The growth temperatures were graded from 520 to 490°C and 505 to 490°C, respectively. They were defined as samples F and G, respectively. Since the total thickness of the InAlAs MBL was maintained to be 1.9 μm, the higher the initial indium content, the lower the mismatch grading rate of the continuously graded $In_yAl_{1-y}As$ buffer, as shown in **Figure 6(a)**. The mismatch grading rates for samples E, F, and G were 1.08, 0.702, and 0.312% μm^{-1}, respectively.

By using this buffer scheme, it was found that RT PL intensity of $In_{0.83}Ga_{0.17}As$ layer was enhanced in sequence from E to G as shown in **Figure 6(b)**, indicating a promoted optical quality of the absorption layer. For the mesa type devices in the diameter size of 200 μm, the dark current was deceased along with the increase of initial In content y from 0.52 to 0.68 and 0.77 under low reverse bias condition. At a reverse bias of −10 mV, the dark current halves for the sample G with respect to that of the sample E at 300 K, as shown in **Figure 6(c)**. This validated the suppression effects of one-step continuously graded $In_yAl_{1-y}As$ MBL on the TDs.

2.3. Strain gradient and composition overshoot in the metamorphic buffer layer

An ideal buffer cannot only restrict the misfit dislocations in the inactive region and reduce the TDD in the absorption layer but also immensely reduce the residual lattice strain in the

http://dx.doi.org/10.5772/intechopen.70259

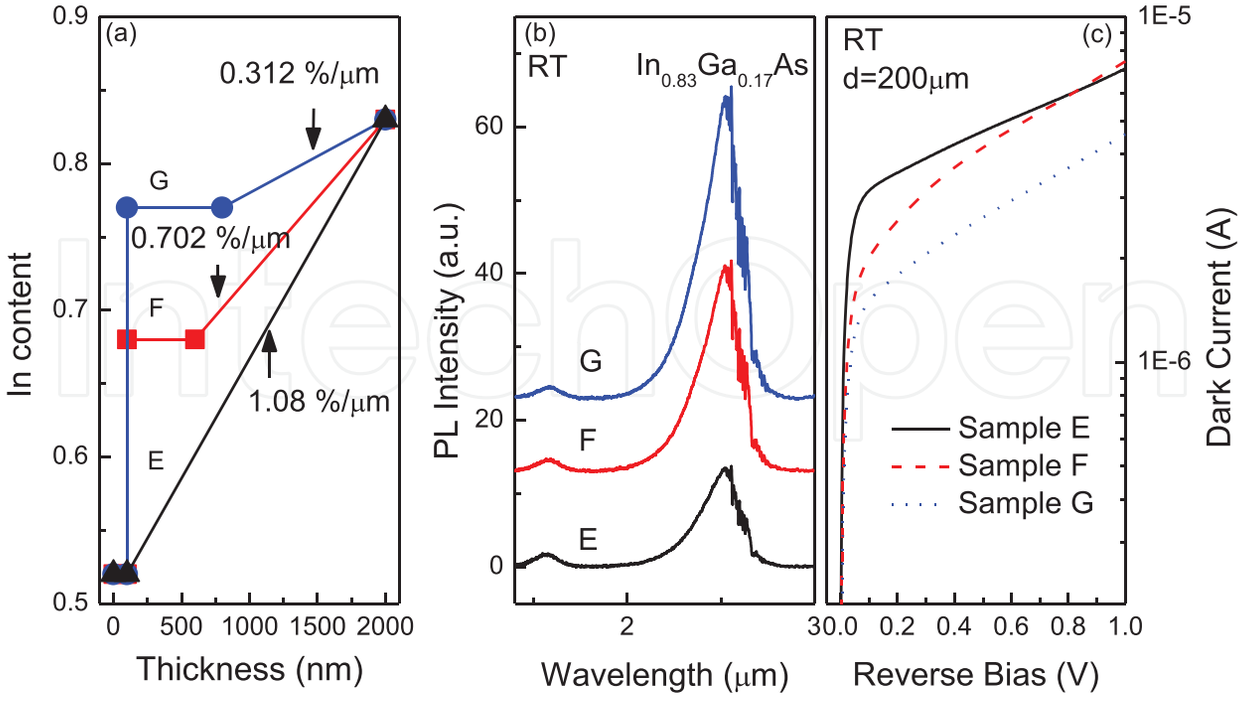

Figure 6. (a) In content vs. the grown thickness, (b) RT PL spectra, and (c) measured I-V characteristics of samples E, F, and G. Reprinted with permission from Elsevier.

epilayer. The strain gradient is proportional to the compositional grading rate in a linearly graded MBL. In this section, 100-nm thin $In_{0.8}Ga_{0.2}As$ layers were grown atop on the 1.6 μm and 0.6 μm linearly graded $In_xGa_{1-x}As$ MBLs on InP, which were defined as samples A and B, respectively. Since the lattice mismatch between the $In_{0.8}Ga_{0.2}As$ layer and the InP substrate is about +1.86%. The strain gradients correspond to be around +1.2% μm^{-1} and +3.1% μm^{-1}, for samples A and B, respectively. The In composition profiles versus growth thickness for the two samples were shown in **Figure 7**. The effects of strain gradient on the surface, structural, and optical properties of the $In_{0.80}Ga_{0.20}As$ metamorphic structures were investigated [25].

The results show that although lower strain gradient caused a slightly rougher surface of the structure shown in **Figure 8**, but it also brought about a larger degree of lattice relaxation and a less residual strain in the top $In_{0.8}Ga_{0.2}As$ layer. **Figure 9** shows the measurement of high-resolution XRD (HRXRD) reciprocal space mapping (RSM). Some results were extracted from the RSM and listed in **Table 2**.

The peaks of the top $In_{0.80}Ga_{0.20}As$ layer of sample A are stronger than that of sample B in both (0 0 4) and (2 2 4) reflections, indicating higher lattice quality of sample A. The lattice relaxation degree is 82.5% for sample A and 77.8% for sample B, respectively. Correspondingly, the residual strain of sample A is smaller than that of sample B. Therefore, it can be concluded that the use of lower strain gradient in the linearly graded MBL is beneficial to the lattice relaxation and the release of residual strain. In addition, a nearly fully strained thin top layer of the structure was observed, indicating a two-step relaxation procedure of the linearly graded MBL as predicted by the Tersoff's model [26]. However, it is still not sufficient to achieve a full relaxation even in the linearly graded $In_xGa_{1-x}As$ MBL with a mismatch

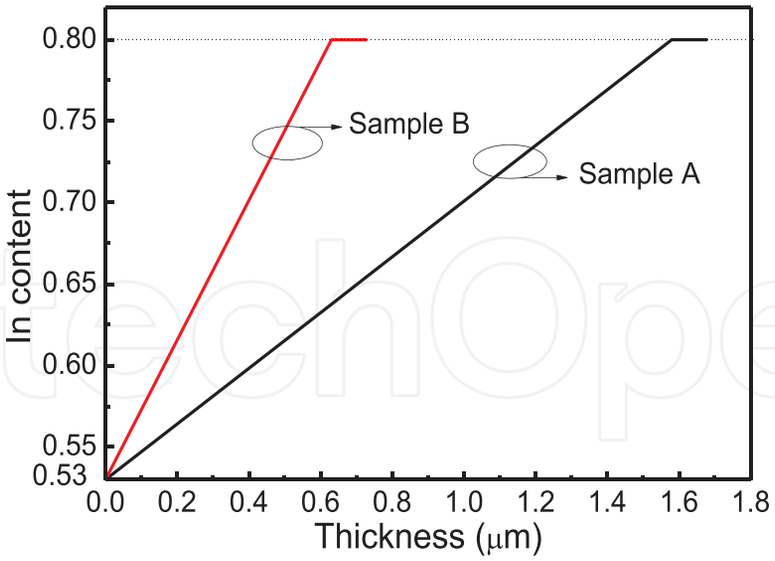

Figure 7. The indium composition versus growth thickness for the two samples. Reprinted with permission from IOP.

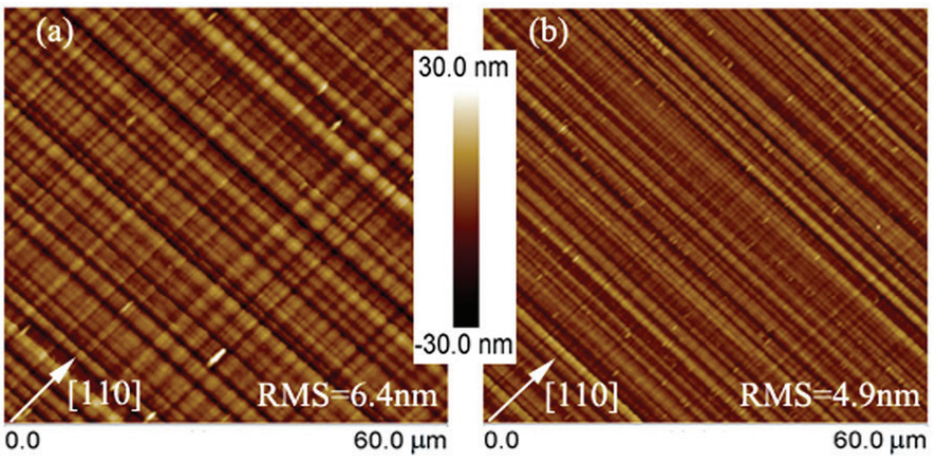

Figure 8. AFM images of (a) sample A and (b) sample B. Reprinted with permission from IOP.

grading rate of 1.2% μm^{-1} in our experiments. Therefore, to further increase the lattice relaxation degree, composition "overshoot" in the MBL should be introduced.

It was proposed that a dislocation-free portion will be formed when the thickness of the buffer is excess of a value of in the linearly graded buffer. The value of Z_c can be expressed as [27]:

$$Z_c = W - (2\lambda/bc\,\varepsilon')^{1/2} \quad (1)$$

where W is the total thickness of the buffer, λ is the energy per unit length of the dislocation, c is the appropriate elastic constant for biaxial strain, b is the misfit component of the Burgers vector of dislocation, and ε' is the strain gradient. The residual strain in this dislocation-free portion can be given by:

http://dx.doi.org/10.5772/intechopen.70259

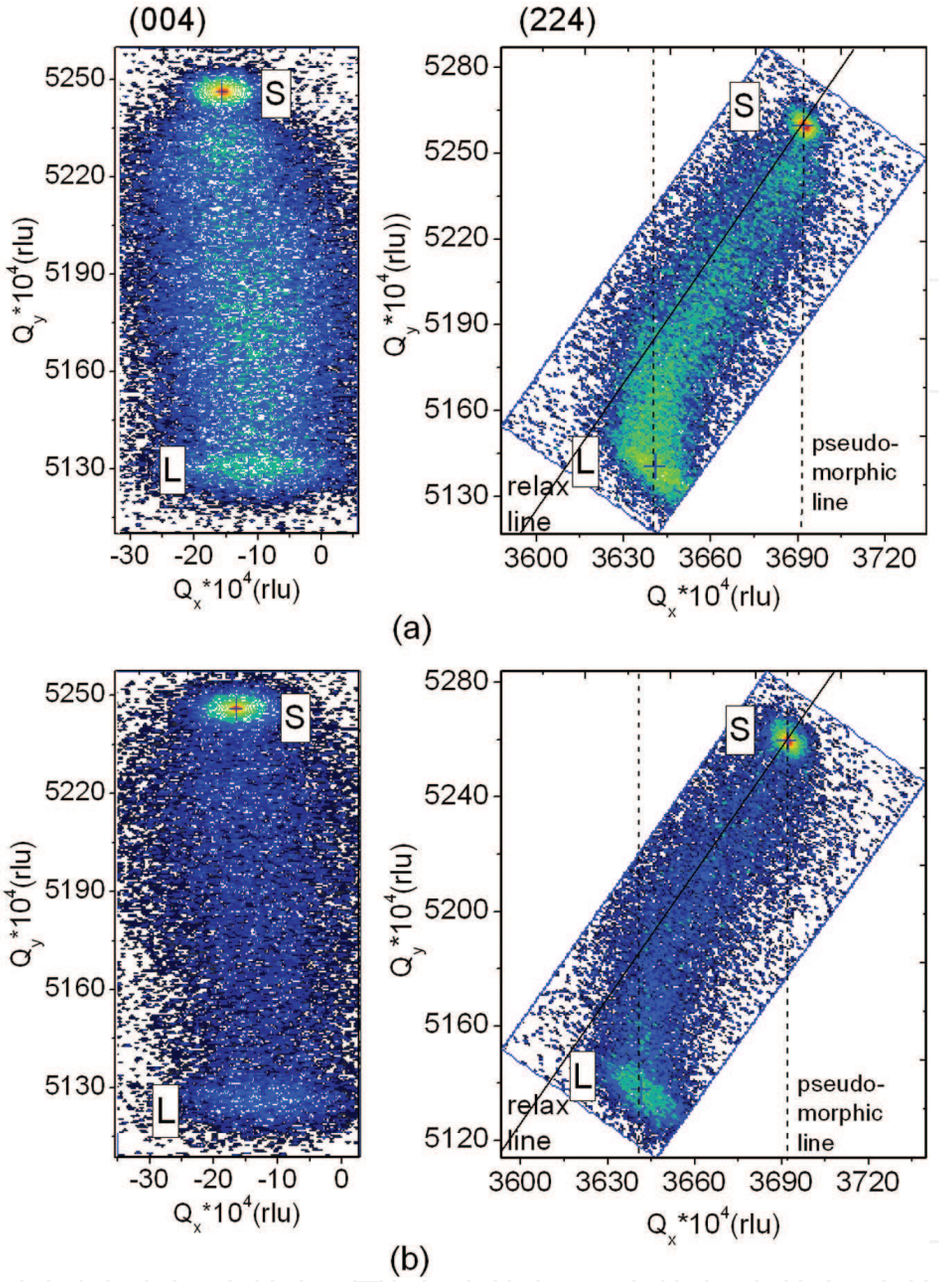

Figure 9. HRXRD RSMs of (a) sample A and (b) sample B. Reprinted with permission from IOP.

Samples	Bulk mismatch (%)	Indium content	Relaxation degree (%)	Parallel mismatch (%)	Perpendicular mismatch (%)	Residual strain (10^{-3})	
						XRD RSM	Tersoff's model
M	1.907	0.806	82.5	1.573	2.322	−3.27	−4.4
N	1.885	0.803	77.8	1.466	2.364	−4.11	−7.0

Table 2. Results extracted from the RSM measurements (reprinted with permission from IOP).

$$\bar{\varepsilon} = W\varepsilon' - Z_c\varepsilon' = (2\lambda\varepsilon'/bc)^{1/2} \quad (2)$$

Therefore, in the linearly graded buffer, an "overshoot" of the mismatch by an amount is needed to make the graded buffer be lattice matched to the following layers. Therefore, to judge this hypothesis, two sets of $In_{0.78}Ga_{0.22}As/In_{0.78}Al_{0.22}As$ quantum wells (QWs) and $In_{0.84}Ga_{0.16}As$ PD structures with and without compositional overshoot in the linearly graded InAlAs MBLs were grown. The effects on the material properties and the lattice relaxation degree have been investigated in detail [28].

As shown in **Figure 10**, the QW structures consist of a 100-nm-thick InP buffer, a 1.7-μm-thick linearly graded $In_xAl_{1-x}As$ MBL, and a three periods of $In_{0.78}Ga_{0.22}As/In_{0.78}Al_{0.22}As$ QWs. The thicknesses of well and barrier layers are 10 and 12 nm respectively, as shown in **Figure 10(a)** and **(b)**. The In composition x in the $In_xAl_{1-x}As$ buffer of this structure was graded from 0.52 to 0.78 for sample 1 and from 0.52 to 0.82 for sample 2. For the $In_{0.84}Ga_{0.16}As$ PD structures, the In composition x in the $In_xAl_{1-x}As$ buffer was designed grading from 0.52 to 0.84 for sample 3 and from 0.52 to 0.88 for sample 4, as shown in **Figure 10(c)** and **(d)**, respectively. Therefore, compositional overshoot of about 0.04 was introduced in the end of the $In_xAl_{1-x}As$ MBLs of samples 2 and 4.

From the AFM, PL, and HRXRD RSM measurement results shown in **Figure 11**, **Figure 12**, and **Table 3**, respectively, we have concluded that the use of compositional overshoot in the InAlAs MBLs not only reduces the surface roughness but also enhances the optical quality and the lattice relaxation degree for both QW and PD structures.

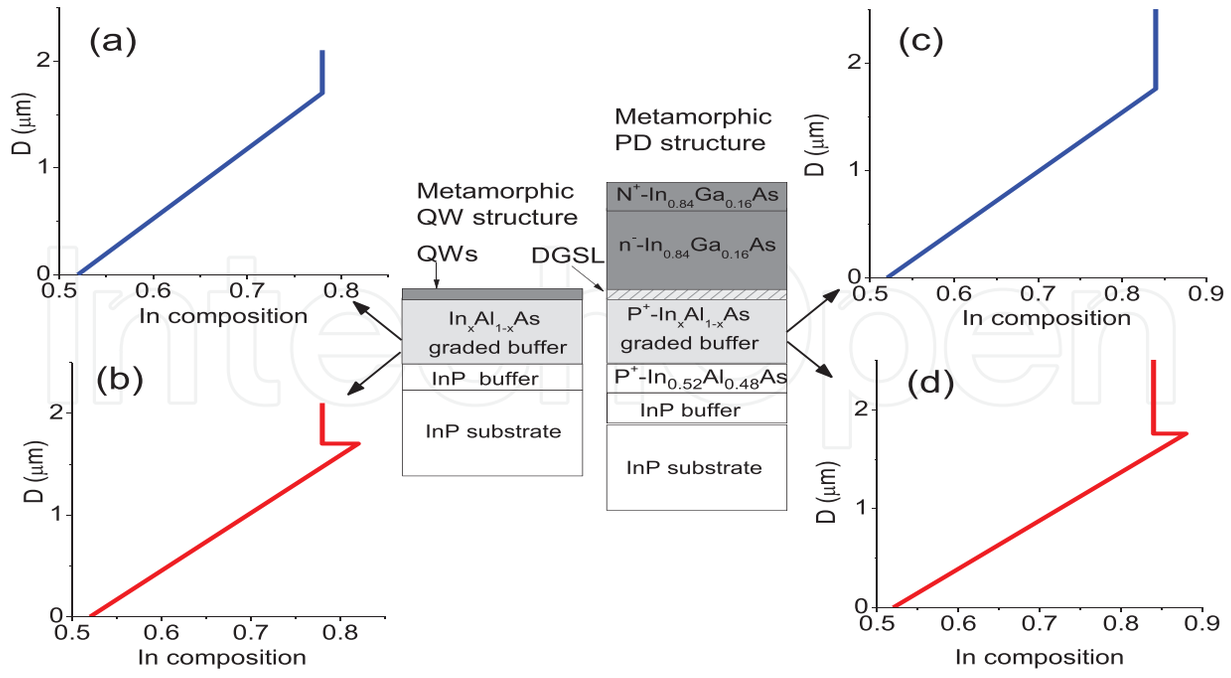

Figure 10. The indium composition profiles in the InAlAs buffer and schematic structures of samples (a) 1, (b) 2, (c) 3, and (d) 4, respectively.

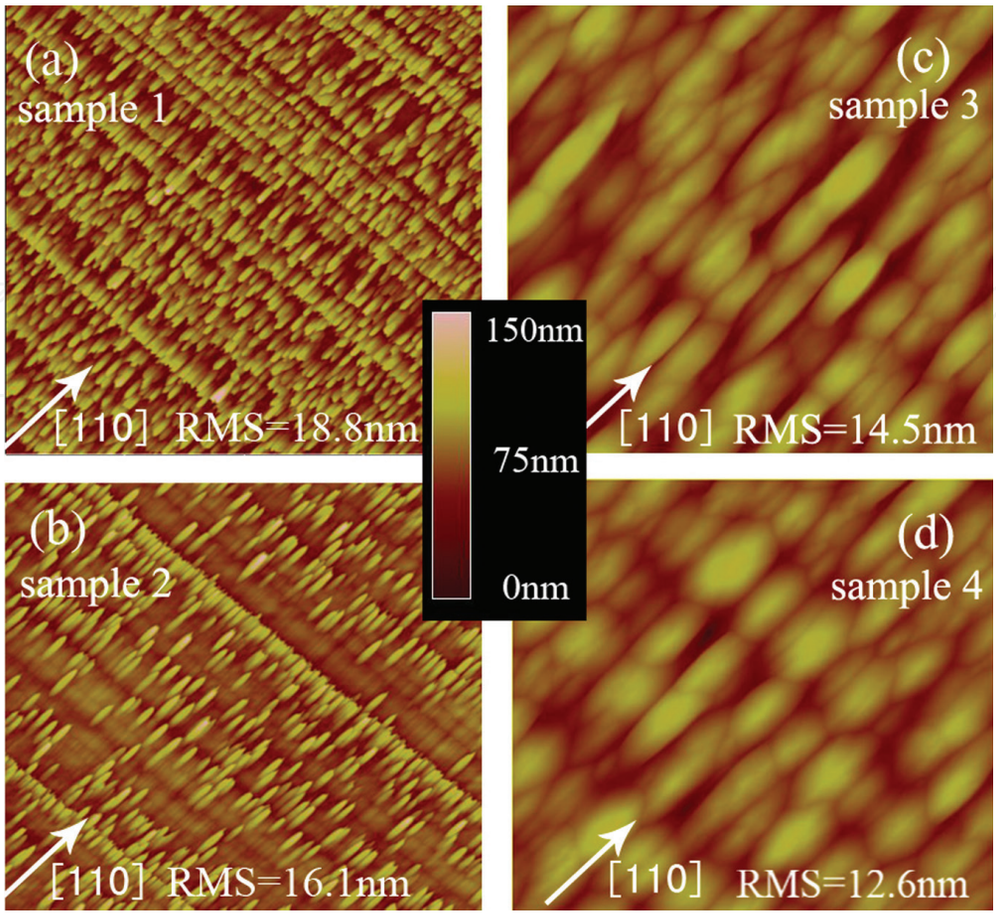

Figure 11. AFM images of (a) sample 1, (b) sample 2, (c) sample 3, and (d) sample 4.

2.4. Adoption of DA for dislocation restriction in the metamorphic buffer layer

Recently, it was confirmed that the insertion of InAs/$In_{0.52}Al_{0.48}As$ DA intermediate layer in the InAlAs MBL can restrain the TDs effectively and improve the structural and optical qualities of the lattice-mismatched system [29].

By alternating the epitaxy of two or more thin layers, DA intermediate layers can be formed. They are expected to reduce the strain energy, restrain the three dimensional (3D) growth, and increase the critical thickness. If the total thickness of one period is set to be d, the needed composition z of the DA layer can be achieved by adjusting the thickness of each thin layer in each period (d_i) through the equation:

$$\sum_{i=0}^{n} \frac{d_i \times m}{d} = z \tag{3}$$

n is the total number of thin layers and m is the composition in each thin layer. These layers are so thin that they would intermix with each other significantly.

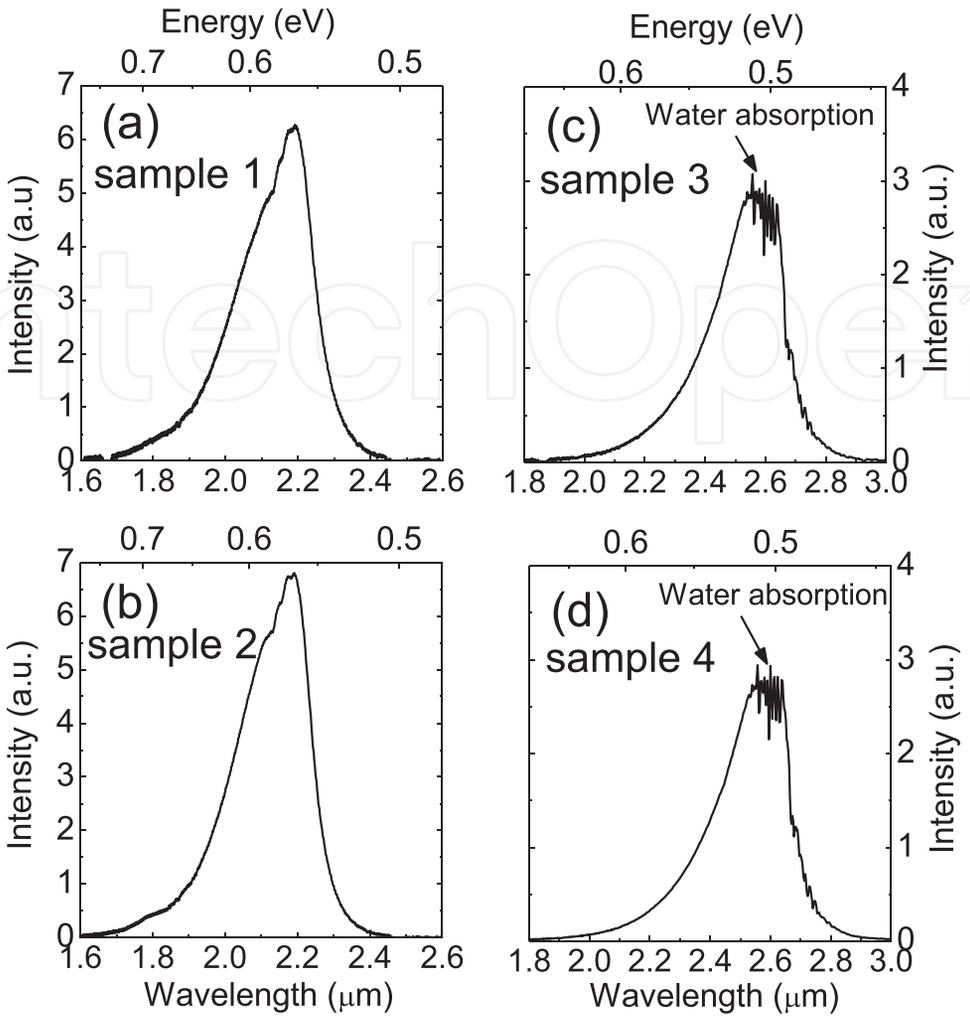

Figure 12. The RT PL spectra of (a) sample 1, (b) sample 2, (c) sample 3, and (d) sample 4.

Samples	Indium content	Cubic mismatch (%)	Parallel mismatch (%)	Perpendicular mismatch (%)	Relax. Degree (%)	Residual strain (10^{-3})
1	0.774	1.675	1.459	1.510	87.2	−2.13
2	0.781	1.730	1.716	2.006	96.5	−0.60
3	0.838	2.125	2.069	2.324	97.4	−0.54
4	0.840	2.136	2.095	2.288	99.4	−0.45

Table 3. Results extracted from RSM measurements of samples 1–4.

As shown schematically in **Figure 13(a)**, two $In_{0.8}Al_{0.2}As/In_{0.8}Ga_{0.2}As$ QW structures were grown on linearly graded InAlAs MBL on InP. As a reference, the In composition x in sample A was continuously graded from 0.52 to 0.8. For sample B, two $In_yAl_{1-y}As$ DA intermediate layers of about 100 nm were inserted into the graded InAlAs MBL, with a separation of every

http://dx.doi.org/10.5772/intechopen.70259

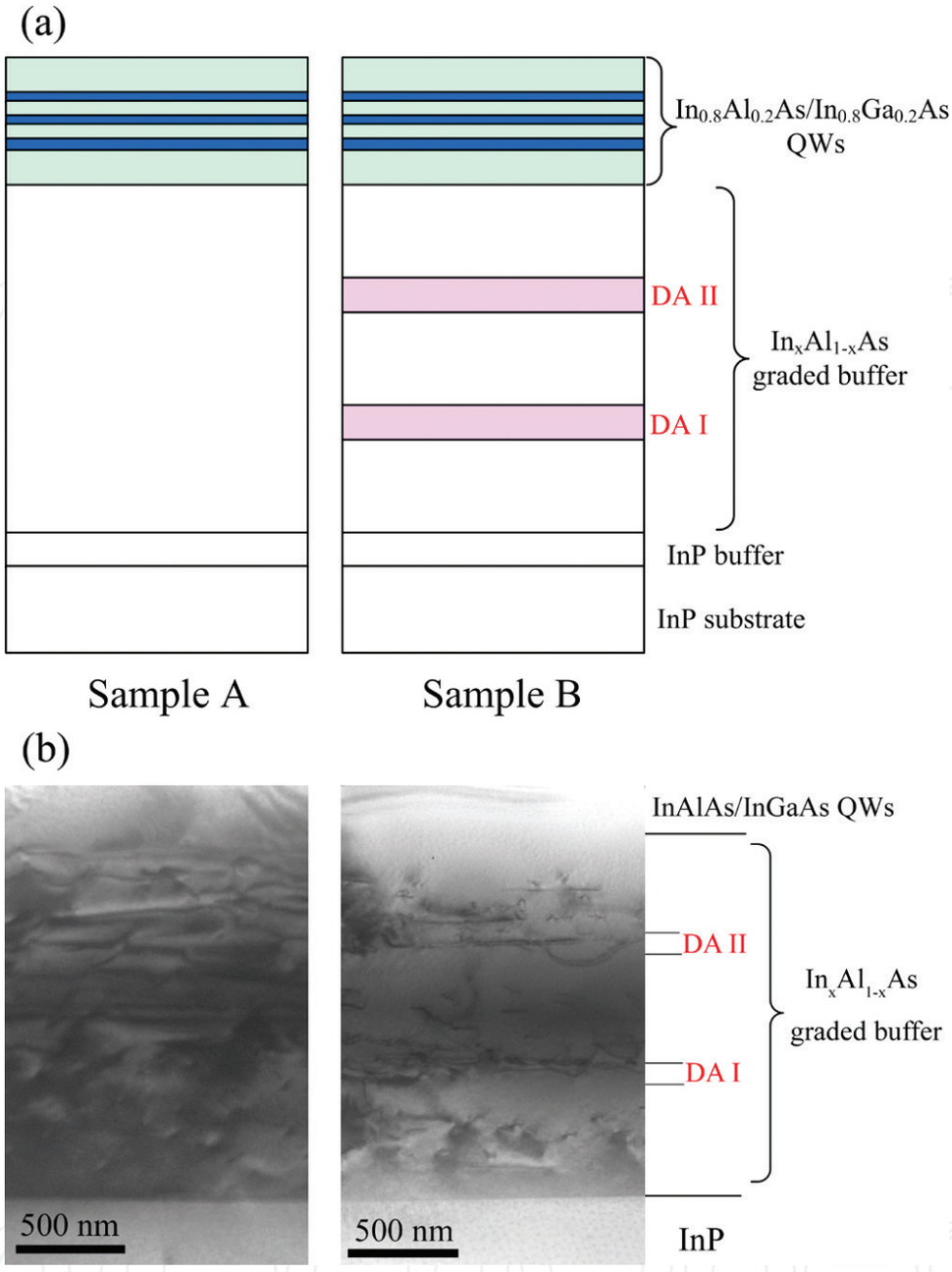

Figure 13. (a) Schematic design structure and (b) XTEM images of the samples. Reprinted with permission from IOP.

500 nm $In_xAl_{1-x}As$ buffer. The In composition of the intermediate layer, y, was designed to be the same as the composition in the inserted positions of the buffer, i.e., y = 0.62 and 0.71 for DA intermediate layers I and II, respectively. The DA layers were formed by the alternating epitaxy of very thin InAs and $In_{0.52}Al_{0.48}As$ layers. The thickness d of a period including one InAs layer and one $In_{0.52}Al_{0.48}As$ layer was 1 nm. The thicknesses of InAs (d_1) and $In_{0.52}Al_{0.48}As$ (d_2) in each period were adjusted to achieve the equivalent In composition y and obtained from the equation:

$$\begin{cases} \dfrac{d_1 + d_2 \times 0.52}{d} = y \\ d_1 + d_2 = d \end{cases}$$

d_1 and d_2 are so small that a considerable material intermixing is expected to occur between the two layers since that the thinnest layer is a submonolayer, and the thickest layer is only about two monolayers (MLs). After the growth of the MBL, three 10-nm $In_{0.8}Ga_{0.2}As$ QWs sandwiched by $In_{0.8}Al_{0.2}As$ barriers were grown. The thickness was 12 nm for the $In_{0.8}Al_{0.2}As$ barrier between the two wells and 100 nm for the first and last barriers.

The measurement results were shown in Figures **13(b)–16**. Although the insertion of InAs/$In_{0.52}Al_{0.48}As$ DA intermediate layers caused a slightly decrease of lattice relaxation degree listed in **Table 4**, the TDD has been decreased immensely in the following InAlAs MBLs as shown in the XTEM images of **Figure 13(b)**, and both the PL and AFM RMS have been improved markedly, indicating the positive effect of the DAs on the structural and optical qualities. However, to maximize these effects, the composition, number, and thickness of the DA should be further optimized.

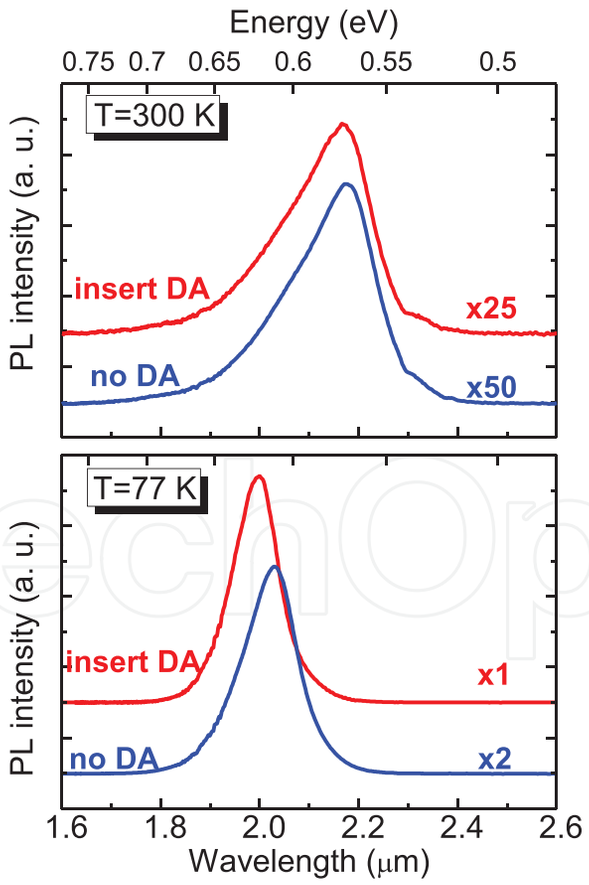

Figure 14. PL spectra of the samples at 300 and 77 K. Reprinted with permission from IOP.

http://dx.doi.org/10.5772/intechopen.70259

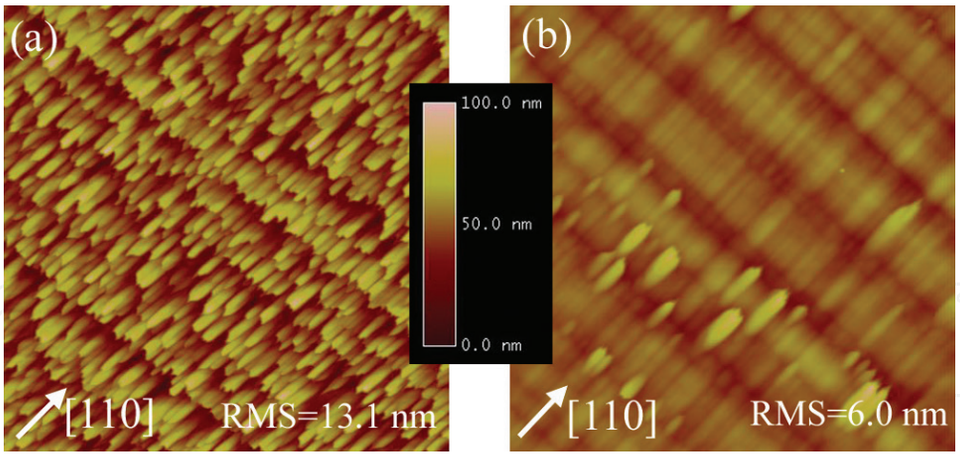

Figure 15. 20 × 20 μm² AFM surface images of (a) sample A and (b) sample B. Reprinted with permission from IOP.

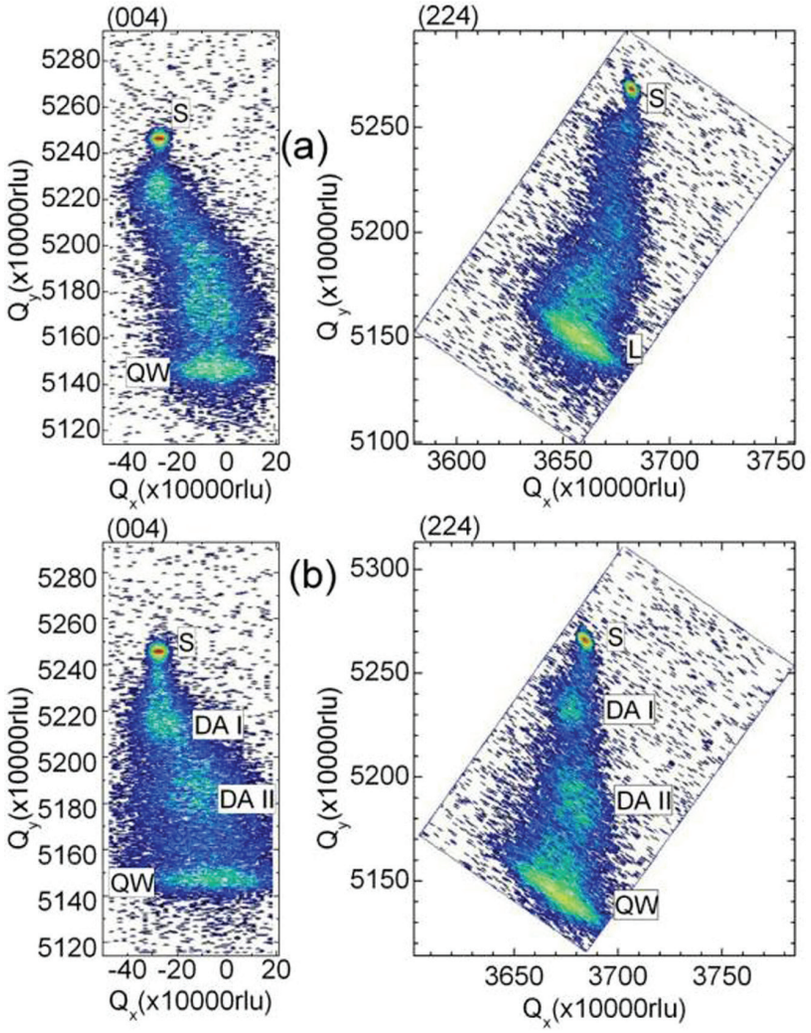

Figure 16. HRXRD RSMs of (a) sample A and (b) sample B. Reprinted with permission from IOP.

Sample	Epitaxy layers	Indium content (y)	Degree of relaxation, R (%)	Residual strain, ε (10^{-3})
A	QW structure	0.760	82.7	−3.5
	QW structure	0.736	70.2	−4.3
B	DA II	0.653	67.1	−2.9
	DA I	0.580	54.9	−1.8

Table 4. Results of XRD RSM measurements (reprinted with permission from IOP).

3. Trials to move $In_{0.83}Ga_{0.17}As$ PD from InP to GaAs substrate

3.1. Comparison of GaAs- and InP-based $In_{0.83}Ga_{0.17}As$ PDs with different lattice mismatches

Currently, most of the wavelength-extended InGaAs PD structures were grown on the InP substrate [2]. Even if a larger lattice mismatch will be introduced, GaAs may still be an attractive substrate for fabrication of InGaAs PDs with large size epitaxial wafers as well as FPAs with more pixels for the advantages of robustness, lower cost, and larger size. However, there are few attempts to transfer $In_xGa_{1-x}As$ ($x > 0.53$) PDs from InP to GaAs substrate.

In our recent researches, two $In_{0.83}Ga_{0.17}As$ PD structures with continuously graded InAlAs MBL were grown on (1 0 0)-oriented S-doped InP or GaAs epi-ready substrates by GSMBE [30]. In this way, the lattice mismatch will increase from +2.1 to +5.9% for $In_{0.83}Ga_{0.17}As$ on GaAs compared to that on InP. The growth condition of InP-based $In_{0.83}Ga_{0.17}As$ PD structure was the same as that in the previous study. For the deposition of the GaAs-based $In_{0.83}Ga_{0.17}As$ PD structure, the InAlAs MBL started with a 0.1-μm-thick highly Si-doped N^+ $In_{0.1}Al_{0.9}As$ layer grown at 530°C, followed by a 1.9-μm-thick compositionally graded $In_xAl_{1-x}As$ layer with In composition x graded from 0.1 to 0.87, and the substrate temperature graded from 530 to 460°C. The mismatch grading rate of 3.1% μm^{-1} for sample A was larger than that of 1.1% μm^{-1} for sample B. Then, a 0.65-μm $In_{0.83}Al_{0.17}As$ template was grown at 460°C in the end of the graded buffer. The growth temperatures of the InGaAs absorption layer and the InAlAs cap layer were 490°C, and the doping level in each layer of both structures was kept uniform. They were renamed as samples S and P for GaAs-based and InP-based $In_{0.83}Ga_{0.17}As$ PD structures, respectively. Their features have been evaluated on both material qualities and device performances.

As the AFM images shows in **Figure 17**, typical anisotropic features of the surface are detected along the [1 1 0] or [1 −1 0] direction in both samples. While the oval-like defects on the surface of sample S seem more distinct, and the undulations of the pattern are larger than those of sample P. The RMS roughness values are 11.3 nm and 4.8 nm for samples S and P, respectively, as shown in **Figure 17**. The relatively smaller RMS value of surface roughness indicates a better crystalline quality of InP-based $In_{0.83}Ga_{0.17}As$ PD structure. The results of measured symmetric (0 0 4) and asymmetric (2 2 4) reflection RSMs (not shown here) showed that

http://dx.doi.org/10.5772/intechopen.70259

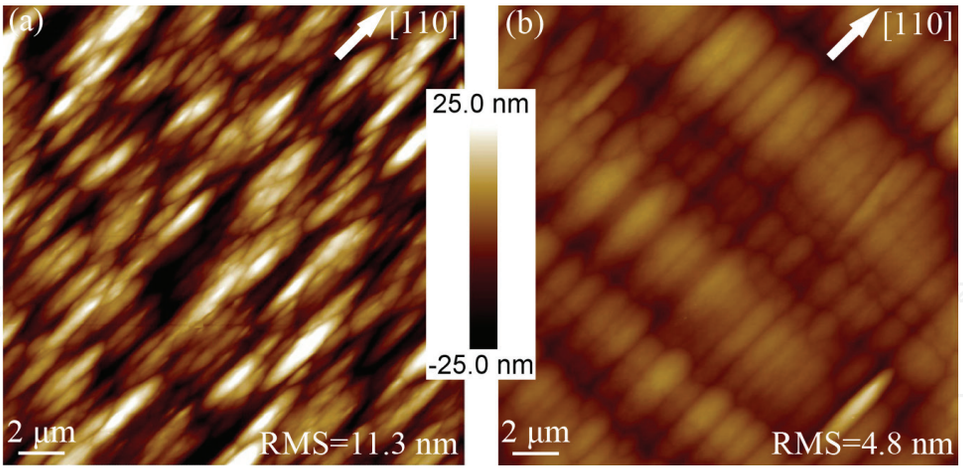

Figure 17. AFM images of (a) sample S, and (b) sample P. The scan area is 20 × 20 μm². Reprinted with permission from Elsevier.

though high lattice relaxation degrees were acquired in both structures, a relatively higher residual strain was observed in the GaAs-based $In_{0.83}Ga_{0.17}As$ PD structure than that in the InP-based structure. This implies that the continuously graded $In_xAl_{1-x}As$ MBL with relatively thin thickness could not well accommodate the relatively higher lattice mismatch between $In_{0.83}Ga_{0.17}As$ and GaAs.

From XRD measurement shown in **Figure 18(a)**, the intensity ratio of epilayer/substrate for sample S is much smaller than that of sample P. Moreover, the FWHM value of the $In_{0.83}Ga_{0.17}As$

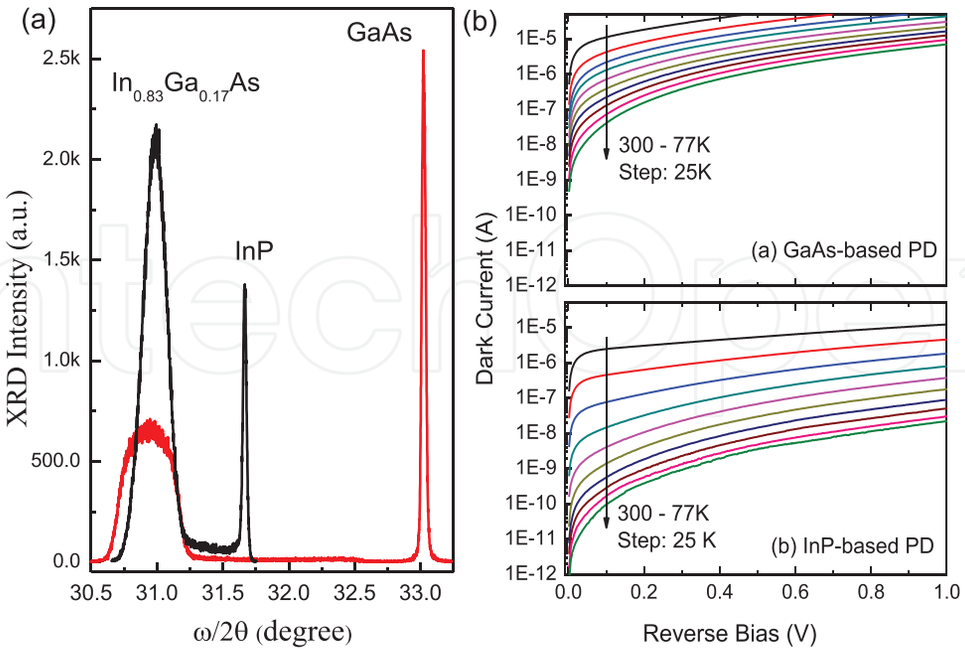

Figure 18. (a) High-resolution (0 0 4) $\omega - 2\theta$ XRD scan curves, and (b) temperature-dependent reverse I-V characteristics of the two samples. Reprinted with permission from Elsevier.

layer of sample S is much larger than that of sample P with values of 1638 and 644 arcsec, respectively. These suggests that the crystal quality of the $In_{0.83}Ga_{0.17}As$ grown on the GaAs substrate is not so good as that grown on the InP substrate with a higher lattice mismatch by using the same type of MBL. This verified one of the conclusions in our previous work [31] that full relaxation and favorable optical property of the InGaAs layer could not occur for the PD wafers with a mismatch grading rate of 2.4% μm^{-1} or above but occur for the wafers with a mismatch grading rate of about 1.2% μm^{-1} or lower.

Correspondingly, quite different temperature dependent I-V characteristics of the two PD chips with diameter of 300 μm were observed in the temperature range from 77 to 300 K, as shown in **Figure 18(b)**. At reverse bias of −10 mV, the dark currents of 2.28 μA at 300 K and 2.17 nA at 77 K for sample S are much larger than that of 674 nA at 300 K and 3.99 pA at 77 K for sample P, respectively, while the zero bias R_0A of the GaAs-based PD is comparable with that of the InP-based PD at 300 K [32], as shown in **Table 5**. This indicates that via appropriate structural design, GaAs may act as a feasible substrate for replacement of InP for $In_{0.83}Ga_{0.17}As$ PDs in some low-end application area around RT.

To analyze the cause of the different electrical performances of the two samples, XTEM measurement was performed firstly, as shown in **Figure 19**. From the XTEM bright-field images, it is obvious that the majority of misfit dislocations of sample P are mainly localized at the early stage of the continuously graded $In_xAl_{1-x}As$ MBL. Threading dislocations have been prevented from propagating into the $In_{0.83}Ga_{0.17}As$ absorption layer by the continuously graded InAlAs MBL on InP under this strain gradient condition. However, it seems that the effect of the continuously graded InAlAs MBL on GaAs is not so remarkable as that on InP. It can be easily seen that many TDs such as 60° dislocations and 60° dislocation pairs generated in the interface of InAlAs MBL and GaAs substrate of sample S have penetrated through the InAlAs buffer and came into the active region. Roughly calculated from **Figure 19(a)**, the TDD in the absorption layer is more than 10^9 cm^{-2} in sample S, much higher than that of sample P with the TDD estimated to be less than 10^8 cm^{-2}.

Second, deep level transient spectroscopy (DLTS) was measured in the temperature range of 77–300 K using DLS-83D DLTS test system and analyzed using standard techniques for the two samples. **Figure 20** shows the DLTS temperature scan signals using reverse bias voltage $V_0 = -2.0$ V, filling pulse height $V_P = 0.5$ V, and filling pulse duration $t_p = 20$ μs. It is evident that no clear peak can be found in the scan signal of InP-based PD. This indicates a low enough density of electrically active defect in the active region of sample P. By contrast, a large electron trap peak around 275 K is clearly observed in that of sample S. Temperature scans with other three lock-in frequencies have also been made and put together to acquire emission

Sample	Relax degree (%)	Residual strain ε (10^{-3})	R@1310 nm (A/W)	η_e@1310 nm (%)	R_0A (Ω cm^2)	$D^*_{\lambda p}$ (cm $Hz^{1/2}$/W)
S	97.5	1.5	0.48	45	3.02	1.30×10^{10}
P	97.7	0.5	0.56	53	9.07	2.25×10^{10}

Table 5. The measured material and device results of samples A and B at 300 K (reprinted with permission from Elsevier).

http://dx.doi.org/10.5772/intechopen.70259

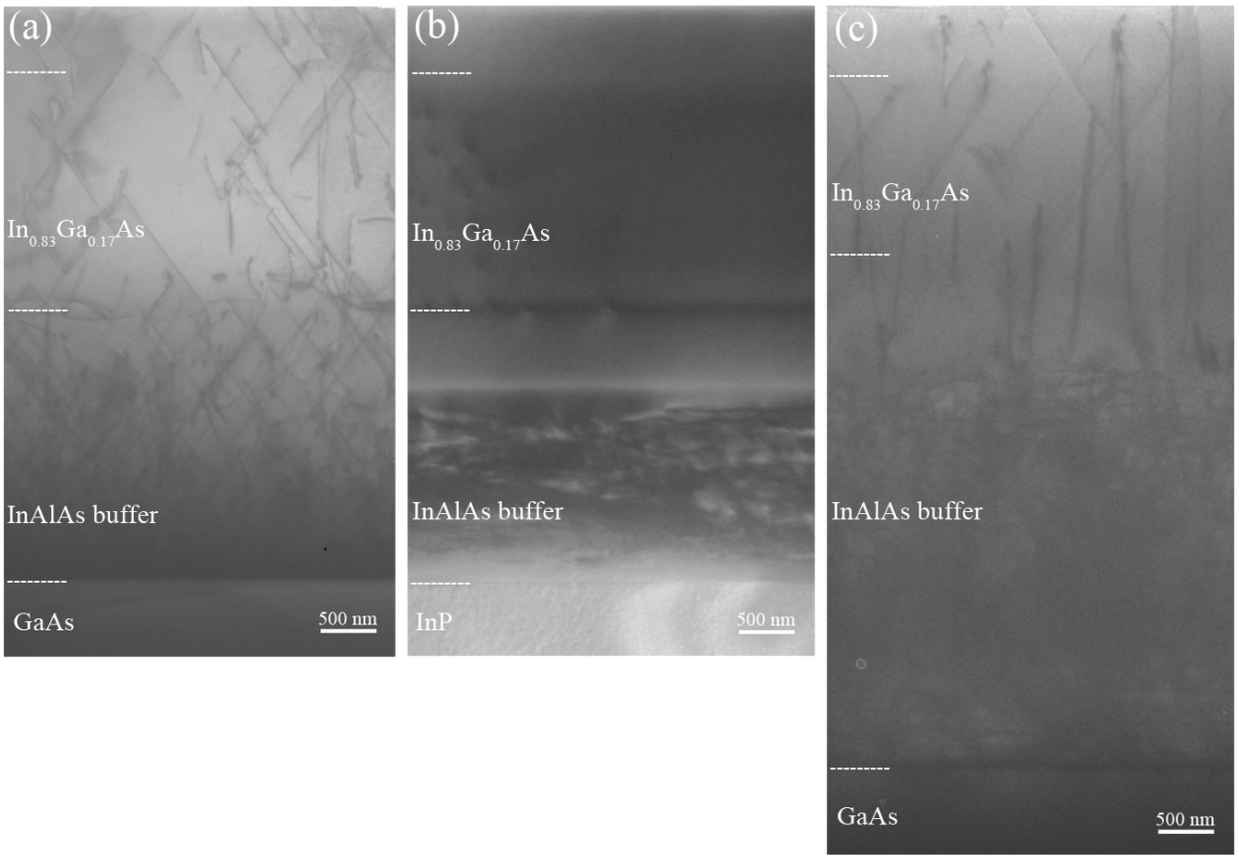

Figure 19. XTEM images of (a) sample S, (b) sample P, and (c) sample S0. Reprinted with permission from Elsevier.

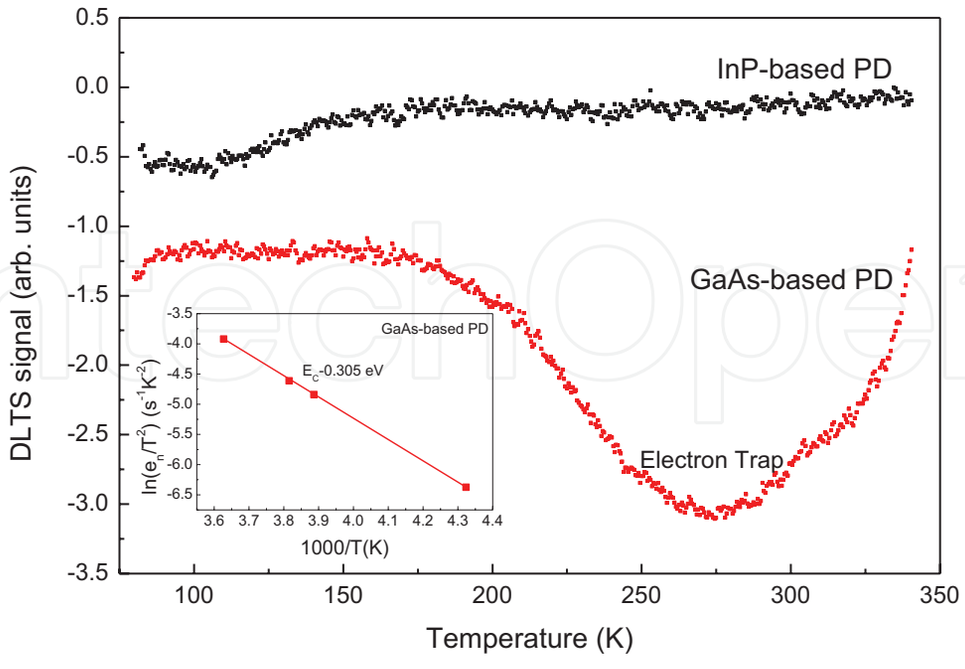

Figure 20. DLTS spectra for the two samples measured at a rate window of 680 Hz. Inset: Arrhenius plot of the deep state observed in GaAs-based PD sample using different lock-in frequencies of 41 Hz, 240 Hz, 320 Hz and 680 Hz. Reprinted with permission from Elsevier.

rate-temperature (e_n-T) data pairs. Then, the standard least-squares fitting for the plot (Arrhenius plot) was applied to extract the trap activation energy and the capture cross-section from the signal peaks. The results are shown in the inset of **Figure 20**. The trap activation energy $E_c - E_T$ = 0.305 eV and the capture cross-section $\sigma_n = 2.25 \times 10^{-18}$ cm^{-2}. This trap will definitely have a deleterious effect on the electrical performance of the PD. Previous literature has reported some deep centers located above the maximum of valence band in lattice-matched $In_{0.53}Ga_{0.47}As$/InP PDs, which were believed to be related with Fe impurities diffused from the Fe-doped substrates to the InGaAs layers [33]. Obviously, the trap occurred here cannot be resulted from Fe impurities because no Fe-doped substrate has been used in this experiment. However, similar traps have been observed in lattice-mismatched $In_{1-x}Ga_xAs$/GaAs hetero-structures [34] and $In_{0.78}Ga_{0.22}As$/InP PDs [35]. Therefore, this 275 K electron trap signal could be associated with the dislocations and point defects in the $In_{0.83}Ga_{0.17}As$ layer because of the even higher lattice mismatch on GaAs compared to that on InP. Since the trap level observed here locates near the center of the bandgap, it is considered that the trap-assisted tunneling current could be the main source of the large dark current in the GaAs-based PD at low temperature range.

On the other hand, the dark current could be expressed by using the thermal activation energy E_a and temperature T as $I_d \sim \exp(-E_a/kT)$ at a fixed reverse bias voltage, where $E_a = E_g/n$, E_g, and n are the band gap energy and the ideal factor, respectively. Therefore, to see the temperature-dependent characteristics of the dark current, Arrhenius plots of the dark currents at −10 mV are made for both samples, as shown in **Figure 21**. For the InP-based PD, near room temperature E_a is almost equivalent to the band gap energy of $In_{0.83}Ga_{0.17}As$ (E_g = 0.48 eV).

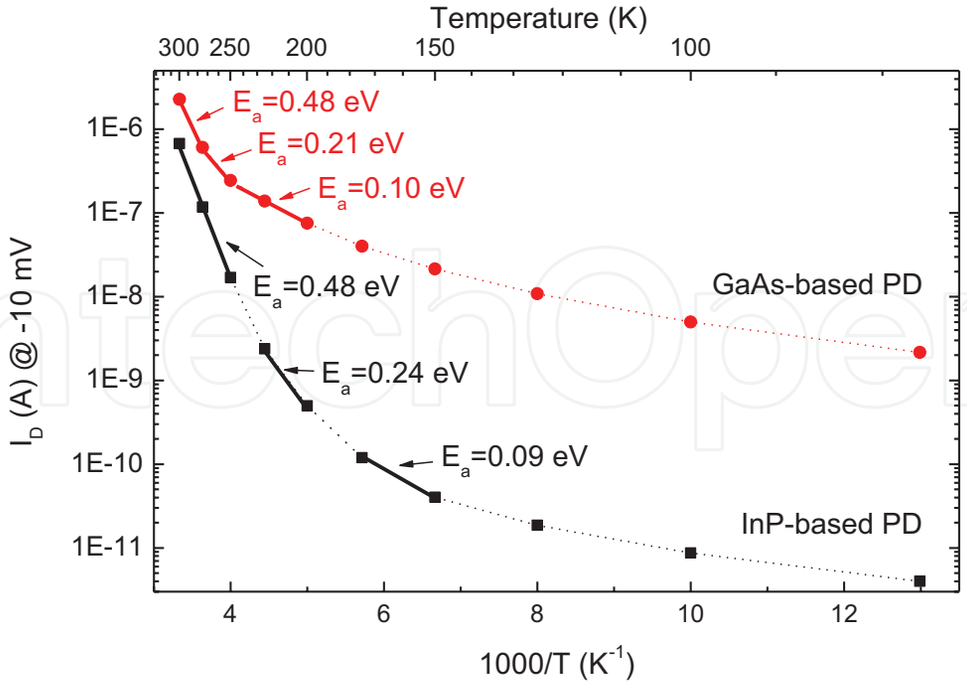

Figure 21. Arrhenius plots of the dark current at −10 mV versus reciprocal temperatures of GaAs- and InP-based PDs. The activation energies in specific temperature regions are also shown in the figure. Reprinted with permission from Elsevier.

It indicates that the dark current is dominated by the diffusion current (I_{diff}) with temperature ranging from about 225 to 300 K. As the temperature drops, E_a is about 0.24 eV in the temperature range of 175–225 K, that is, the thermal activation energy is about half of the band gap energy of $In_{0.83}Ga_{0.17}As$. It means that the dark current is dominated by the generation-recombination current ($I_{g\text{-}r}$) in this range. As the temperature reduces lower than 175 K, E_a becomes smaller, and thus, the components of trap-assisted tunneling current (I_{tat}) and/or band-to-band tunneling (I_{btb}) start to play an important role. However, it was found that the temperature dependence of E_a in the GaAs-based PD is much stronger than that of InP-based PD. That is, I_{diff} and $I_{g\text{-}r}$ dominate the dark current of the GaAs-based PD in a much smaller temperature region than that of InP-based PD. Alternatively, the majority component is tunneling current at temperatures lower than 250 K, when E_a is much less than the band gap of $In_{0.83}Ga_{0.17}As$. This explained the higher dark current of the GaAs-based PD at the low-temperature region shown in **Figure 18(b)**. The large component proportion of tunneling current could be due to a high TDD in the active region caused by the relatively high lattice mismatch between $In_{0.83}Ga_{0.17}As$ and GaAs [30]. This agrees well with the DLTS results.

To further optimize the GaAs-based PD structure and understand the strain relaxation mechanism with such a relatively high lattice mismatch, it is necessary to increase the buffer thickness and thus decrease the strain gradient of the continuously graded $In_xAl_{1-x}As$ MBL. Therefore, as a comparison, an $In_{0.83}Ga_{0.17}As$ PD structure (renamed as sample S0) with a 5-μm-thick continuously graded $In_xAl_{1-x}As$ MBL and 1.5-μm-thick $In_{0.83}Ga_{0.17}As$ absorption layer has been also grown on a GaAs substrate. So that the mismatch grading rate in the $In_xAl_{1-x}As$ MBL was lowered to about 1.2% μm^{-1}, close to that used for the $In_xAl_{1-x}As$ MBL on InP substrate. By comparison with samples S and P, the XRD and PL results of sample S0 are really better than those of sample S but still worse than that of sample P. Roughly estimated from the XTEM image of **Figure 19(c)**, the average TDD in the absorption layer of sample S0 is only slightly less than that of sample S but still much larger than that of sample P. In addition, some differences were observed between the two XTEM images of samples S and S0. The 60° dislocations and 60° dislocation pairs, which are dominant in sample S, have been mostly replaced by Lomer (90°) dislocations in sample S0. It would be resulted from reactions of 60° dislocations from different glide systems to form Lomer dislocations on the top of the InAlAs MBL due to a two-dimensional growth mode in the thicker buffer of sample S0 [36, 37]. This means that the lower mismatch grading rate of the MBL has improved the characteristics of the PD structure very limited except for the evolution of the TDs.

Therefore, it is supposed that the composition continuously graded buffer may not be a good strategy for growth of material systems with relatively high lattice mismatch due to a quite low growth rate of the MBE technique. A more suitable thin buffer layer should be exploited, and the metamorphic strategy will be updated accordingly.

3.2. Optimization of InAlAs metamorphic buffer on GaAs with relatively high lattice mismatch

From the discussions above, GaAs-based high In content InGaAs PDs may be not a good choice for practical special application of remote sensing at the low temperature range.

However, it is still valuable to design and develop an appropriate buffer scheme for the device development from material system with relatively high-lattice mismatch.

Since that the way strain is introduced at the initial stage of the MBL has been proved to play a critical role in the final TDD [10]. The strain energy should be released as quickly as possible, and the multiplication of TD must be avoided occurring at the final stage of the buffer layer. Therefore, if we take the accessory advantage of this relatively high lattice mismatch between high In content InGaAs and GaAs, we can promote the nucleation of dispersed TDs at the initial stage of the MBL. Considering that the high In content InAlAs and/or InGaAs will quickly achieve a high relaxation on GaAs due to the small critical thickness. Specifically, for the growth of $In_{0.83}Ga_{0.17}As$ PD on GaAs, we can use the fixed-composition $In_{0.83}Al_{0.17}As$ as MBL to accelerate the release of strain energy and the nucleation of dispersed misfit dislocations at the initial stage of the buffer and thus restrain the misfit dislocation at the interface between $In_{0.83}Al_{0.17}As$ and GaAs. The uniform composition buffer will also reduce the strain gradient at the later stage of the MBL with lattice nearly fully relaxed. We show that this method results in a lower TDD and a smoother surface of the final absorption and cap layer.

In this work, four $In_{0.83}Ga_{0.17}As$ PD structures with different buffer schemes were grown by GSMBE on S.I. (1 0 0)-oriented GaAs epi-ready substrates [38]. Each structure consisted of a 2.5-μm N^+ InAlAs MBL and a 1.5-μm n^- $In_{0.83}Ga_{0.17}As$ absorption layer followed by a 530 nm P^+ InAlAs cap. The detailed buffer schemes for samples GS1, GS2, GS3, and GS4 were listed in **Table 6**. Growth condition was exactly the same as that in our previous study [30]. The strategies of substrate temperature graded from 530 to 460°C, and the uniform temperature of 490 °C were adopted for the deposition of continuously graded $In_xAl_{1-x}As$ and fixed-composition $In_{0.83}Al_{0.17}As$ buffer, respectively. In addition, InAs wetting layer was inserted between the fixed-composition $In_{0.83}Al_{0.17}As$ layer and the GaAs substrate for samples GS3 and GS4 to investigate the effect of interfacial layer on the TD behaviors at the interface.

As shown in **Figure 22**, compared to sample GS1, the cross-hatch pattern in the 2D AFM image of sample GS2 is less pronounced, and smaller diameters of 3D mounds align along the [1 1 0] direction in the 3D AFM image, indicating a smaller residual strain fields on the surface [39]. Thus, the RMS roughnesses of samples GS2–GS4 are a little smaller than that of sample GS1, as summarized in **Table 6**. As well known, when the thickness of the epilayer is beyond the critical value, the misfit strain could relax by introducing misfit dislocation arrays as well as surface undulation [40, 41]. The larger RMS value and larger size of 3D mounds on the structural surface of sample GS1 reflect that the strain-reliving surface roughening is more serious in sample GS1 than samples GS2–GS4.

Figure 23(a) shows the normalized HRXRD rocking curves for (0 0 4) reflections of all samples, which is also related to the TDD and other crystal imperfections [42]. A broader peak located at about 31° of sample GS1 reflects the continuously grading profile of $In_xAl_{1-x}As$ ($x = 0.1 \rightarrow 0.86$) MBL which ultimately combined with the $In_{0.83}Ga_{0.17}As$ peak. While much lower FWHM of $In_{0.83}Ga_{0.17}As$ layers for samples GS2–GS4 mainly due to the thicker fixed-composition $In_{0.83}Al_{0.17}As$ MBL. Though all PD structures exhibited high degree of lattice relaxation, shown in **Table 6**, the improvement of structural surface and crystal quality was believed to be associated with the amelioration of misfit dislocation formation at the

Sample	Buffer scheme	XRD FWHM (arcsec)	Relaxation degree (%)	In composition	AFM RMS (nm)
GS1	2.5 μm $In_xAl_{1-x}As$ buffer, x grades from 0.1 to 0.86	1782	94.8	0.84	11.6
GS2	2.5 μm $In_{0.83}Al_{0.17}As$	544	97.5	0.82	8.1
GS3	5 MLs InAs QDs + 2.5 μm $In_{0.83}Al_{0.17}As$	410	98.3	0.83	8.8
GS4	50 nm InAs + 2.5 μm $In_{0.83}Al_{0.17}As$	511	98.8	0.82	8.6

Table 6. Buffer schemes and measured results for four samples (reprinted with permission from Elsevier).

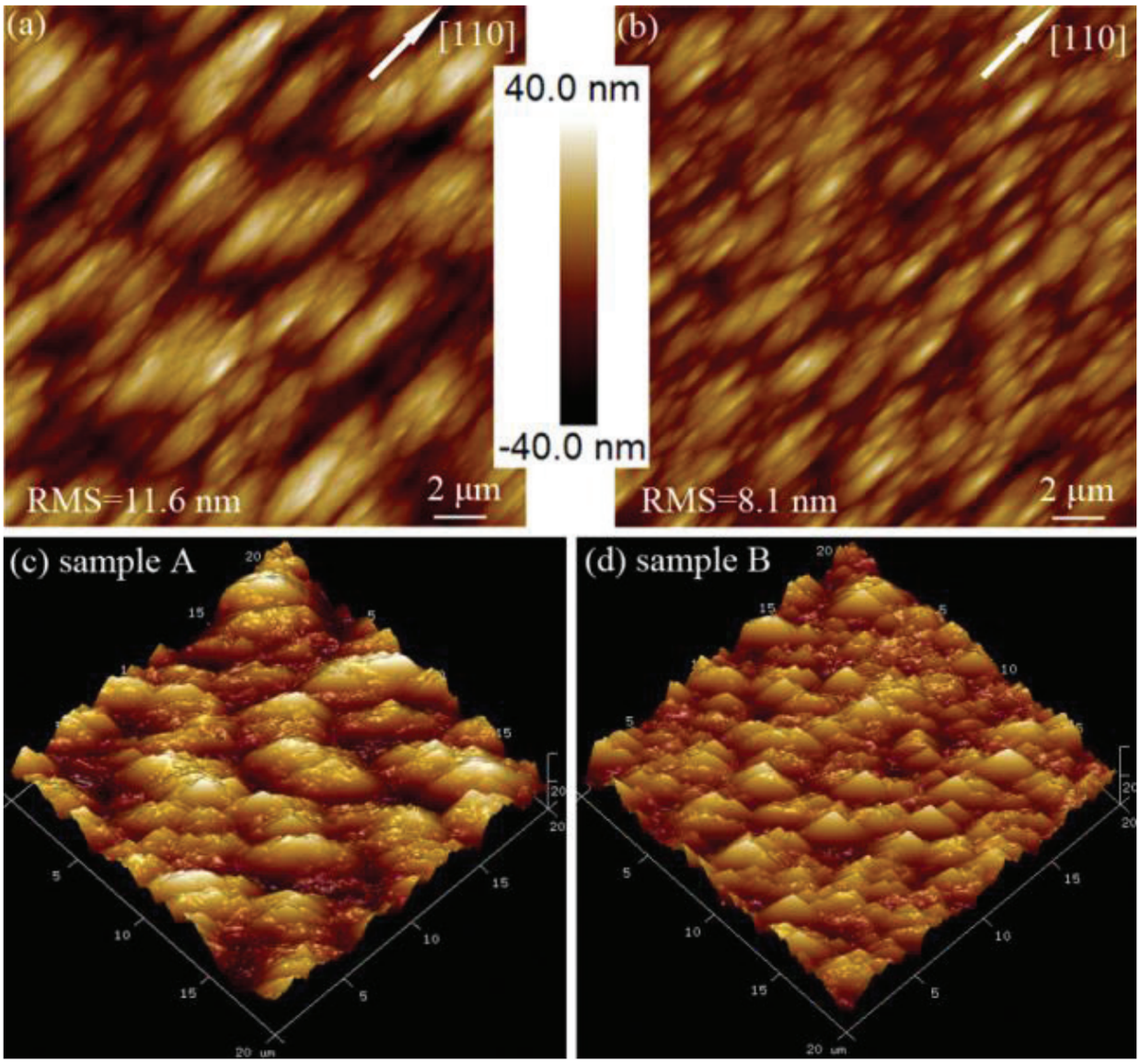

Figure 22. AFM images of samples A and B. The scan area is 20 × 20 μm². Reprinted with permission from Elsevier.

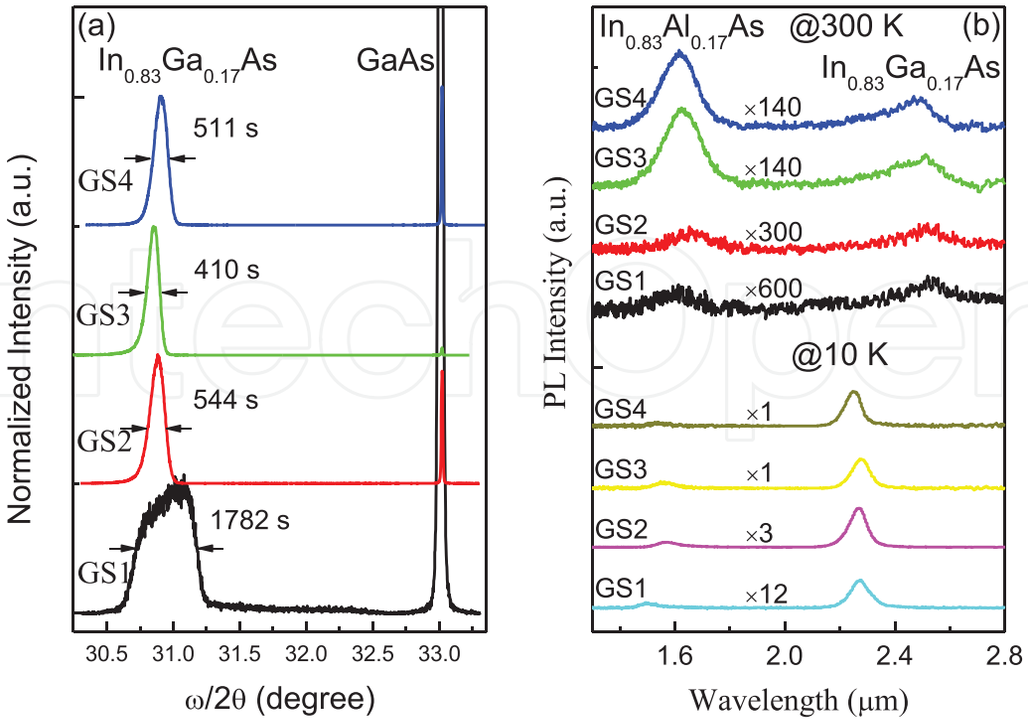

Figure 23. (a) (0 0 4) $\omega - 2\theta$ high resolution XRD patterns. (b) PL spectra at 300 K and 10 K of samples GS1–GS4. Reprinted with permission from Elsevier.

film/substrate interface [43]. This was further demonstrated by sample GS3 with a narrowest FWHM value of 410 arcs by inserting 5 MLs InAs QDs at the $In_{0.83}Al_{0.17}As$/GaAs interface. This indicates that the growth of the QD is beneficial to the dislocation nucleation at the interface and the confinement of misfit dislocations in the inactive region, while the effect is slightly weakened when InAs was thickened and degenerated, resulting in a degraded interfacial quality.

From the PL spectra measured at 300 and 10 K shown in **Figure 23(b)**, we can see that the PL intensity of the $In_{0.83}Ga_{0.17}As$ absorption layers increased in sequence for samples GS1–GS3, meaning that the crystal defect has been suppressed through the substitution of continuously graded $In_xAl_{1-x}As$ MBL by fixed-composition $In_{0.83}Al_{0.17}As$ MBL. The XTEM images of the two typical PD structures were shown in **Figure 24**. For sample GS1, it is notable that the misfit dislocation networks were separated by 0.1 μm from the interface between $In_{0.1}Al_{0.9}As$ and GaAs because of the $In_{0.1}Al_{0.9}As$ layer, and highly intensive dislocation arrays accumulated in the lower area of the $In_xAl_{1-x}As$ grading layer, as shown in **Figure 24(a)**. Many vertical dislocations with long dislocation length, thread from the tangling area through the buffer along the [1 0 0] direction and propagate to the top active region of the PD structure. Strain in this structure released dominantly by surface undulation, which deteriorates the surface morphology of the PD structure and leads to a large RMS roughness. The surface ripple troughs–induced misfit dislocations were generated by gliding of dislocation half loops from the surface through the epilayer [44].

However, the dislocations in the structure of sample GS2 are short, and most of them are not perpendicular to the sample surface, as shown in **Figure 24(b)**. We supposed that $In_{0.83}Al_{0.17}As$ QDs would form at the beginning of growth process of the fixed-composition $In_{0.83}Al_{0.17}As$

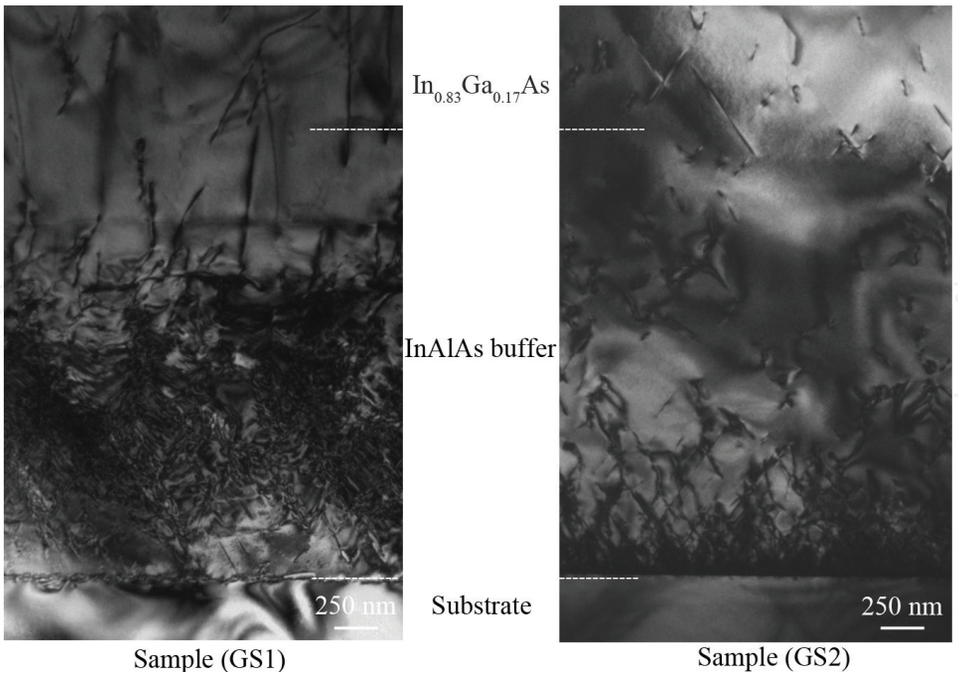

Figure 24. XTEM images of (a) sample GS1 and (b) sample GS2. Reprinted with permission from Elsevier.

layer because of the relatively high-lattice mismatch of 5.9% with respect to GaAs. Therefore, the relaxation process in the fixed-composition buffer of sample GS2 may start with a layer-to-island transition (Stranski-Kranstanov growth mode) after the deposition of a couple MLs of $In_{0.83}Al_{0.17}As$ on GaAs. Then, the large compressive strain can be released by generation and reaction of misfit dislocation networks. Since the initial growth mechanism will also affect the dislocation generation mechanism in the hetero-epitaxy of $In_xGa_{1-x}As$ on GaAs except for the lattice mismatch [10]. The formation of $In_{0.83}Al_{0.17}As$ QDs at the initial stage of the $In_{0.83}Al_{0.17}As$ MBL has indeed played an important role by the formation of high density of nucleation sites [13], which can act as core of misfit dislocations. In this way, the relaxation process is promptly due to the substantial lattice mismatch and most of the misfit dislocations are inhibited to the core areas, which locate close to the $In_{0.83}Al_{0.17}As$/GaAs interface. Therefore, TDs in the buffer of sample GS2 cannot propagate a long distance due to the island growth near the interface. They annihilated much easier by interaction with the point defects existing in the high In content $In_{0.83}Al_{0.17}As$ layer with respect to the $In_xAl_{1-x}As$ MBL of sample GS1. It is expected that the intermediate layer of 5 MLs InAs QD will enhance the dislocation nucleation process at the $In_{0.83}Al_{0.17}As$/GaAs interface because of a higher lattice mismatch between InAs and GaAs. Through appropriate buffer design, fixed-composition $In_{0.83}Al_{0.17}As$ buffer may be a better choice for the growth of metamorphic $In_{0.83}Ga_{0.17}As$ PDs on GaAs substrate.

4. Conclusion

In conclusion, due to the inventions of metamorphic techniques such as, linearly, step, and one-step continuously graded buffer, compositional overshoot, and DA in the growth of

lattice-mismatched material system, the development of InP- and GaAs-based wavelength-extended $In_xGa_{1-x}As$ ($x > 0.53$) photodetectors with relatively high lattice mismatch has achieved remarkable success in SWIR band especially for the applications at higher operation temperatures and robust circumstances. Though GaAs-based $In_{0.83}Ga_{0.17}As$ PD shows large potential in some low-end application area around RT, the high densities of TDs and electron traps in the active region due to the relatively high-lattice mismatch have hindered its development. By designing of abrupt interface and appropriate buffer, the initial dislocation nucleation process may pave a way of development of lattice-mismatched device structures.

Acknowledgements

The authors wish to acknowledge the support of the National Key Research and Development Program of China under Grant No. 2016YFB0402400, the National Natural Science Foundation of China under grant Nos. 61405232, 61675225, and 61605232, and the Youth Innovation Promotion Association CAS under Grant No. 2013155.

Author details

Xing-you Chen*, Yi Gu and Yong-gang Zhang

*Address all correspondence to: xychen@mail.sim.ac.cn

State Key Laboratory of Functional Materials for Informatics, Shanghai Institute of Microsystem and Information Technology, Chinese Academy of Sciences, China

References

[1] Hoogeveen RWM, JvdA R, Goede APH. Mint: Extended wavelength InGaAs infrared (1.0-2.4 μm) detector arrays on SCIAMACHY for space-based spectrometry of the Earth atmosphere. Infrared Physics Technology. 2001;**42**:1-16. DOI: 10.1016/S1350-4495(00)00061-X

[2] Zhang YG, Gu Y. Gas source MBE grown wavelength extending InGaAs photodetectors. In: Betta GFD, editor. Advances in Photodiodes. Croatia: InTech; 2011. pp. 349-376. DOI: 10.5772/13910

[3] Tangring I, Wang SM, Zhu XR, Larsson A, Lai ZH, Sadeghi M. Mint: Manipulation of strain relaxation in metamorphic heterostructures. Applied Physics Letters. 2007;**90**: 071904. DOI: 10.1063/1.2435609

[4] Song YX, Wang SM, Lai ZH, Sadeghi M. Mint: Enhancement of optical quality in metamorphic quantum wells using dilute nitride buffers. Applied Physics Letters. 2010;**97**:091903. DOI: 10.1063/1.3483839

[5] Ji L, Lu SL, Zhao YM, Tan M, Dong JR, Yang H. Mint: Compositionally undulating step-graded $InAs_yP_{1-y}$ buffer layer growth by metal-organic chemical vapor deposition. Journal of Crystal Growth. 2013;**363**:44-48. DOI: 10.1016/j.jcrysgro.2012.09.035

[6] Zhao L, Sun JG, Guo ZX, Miao GQ. Mint: TEM dislocations characterization of In_xGa_{1-x} As/InP (100) (x = 0.82) on mismatched InP substrate. Materials Letters. 2013;**106**:222-224. DOI: 10.1016/j.matlet.2013.04.116

[7] Zhao L, Guo ZX, Wei QL, Miao GQ, Zhao L. Mint: The relationship between the dislocations and microstructure in $In_{0.82}Ga_{0.18}As$/InP heterostructures. Scientific Reports. 2016;**6**:35139. DOI: 10.1038/srep35139

[8] Lubyshev D, Liu WK, Stewart TR, Cornfeld AB, Fang XM, Xu X, Specht P, Kisielowski C, Naidenkova M, Goorsky MS. Mint: Strain relaxation and dislocation filtering in metamorphic high electron mobility transistor structures grown on GaAs substrates. Journal of Vacuum Science and Technology B. 2001;**19**:1510-1514. DOI: 10.1116/1.1376384

[9] Valtuena JF, Sacedon A, Alvarez AL, Izputa I, Calle F, Calleja E, MacPherson G, Goodhew PJ, Pacheco FJ, Garcia R and Molina SI. Mint: Influence of the surface morphology on the relaxation of low-strained $In_xGa_{1-x}As$ linear buffer structures. Journal of Crystal Growth. 1997;**182**:281-291. DOI: 10.1016/S0022-0248(97)00377-1

[10] Chang SZ, Chang TC, Lee SC. Mint: The growth of highly mismatched $In_xGa_{1-x}As$ ($0.28 \leq x \leq 1$) on GaAs by molecular-beam epitaxy. Journal of Applied Physics. 1993;**73**:4916. DOI: 10.1063/1.353809

[11] Chang CA, Serrano CM, Chang LL, Esaki L. Mint: Studies by cross-sectional transmission electron microscope of InAs grown by molecular beam epitaxy on GaAs substrates. Applied Physics Letters. 1980;**37**:538. DOI: 10.1063/1.91977

[12] Zimmermann L, John J, de Weerd M, Slaman M, Nemeth S, Merken P, Borghs S, Van Hoof C. Mint: InGaAs on GaAs extended wavelength linear detector arrays. Proceedings of SPIE. 2001;**4288**:77-84. DOI: 10.1117/12.429396

[13] Song YX, Wang SM, Tangring I, Lai ZH, Sadeghi M. Mint: Effects of doping and grading slope on surface and structure of metamorphic InGaAs buffers on GaAs substrates. Journal of Applied Physics. 2009;**106**:123531. DOI: 10.1063/1.3273492

[14] Jurczak P, Sablon KA, Gutierrez M, Liu HY, Wu J. Mint: 2.5-μm InGaAs photodiodes grown on GaAs substrates by interfacial misfit array technique. Infrared Physics & Technology. 2017;**81**:320-324. DOI: 10.1016/j.infrared.2017.02.001

[15] Gao FL, Wen L, Zhang XN, Guan YF, Li JL, Zhang, SG, Li GQ. Mint: Structural properties of $In_{0.53}Ga_{0.47}As$ epitaxial films grown on Si (111) substrates by molecular beam epitaxy. Thin Solid Films. 2015;**589**:32-37. DOI: 10.1016/j.tsf.2015.04.085

[16] Toikkanen L, Hakkarainen T, Schramm A, Tukiainen A, Laukkanen P, Guina M. Mint: Metamorphic growth of tensile strained GaInP on GaAs substrate. Journal of Crystal Growth. 2010;**312**:3105-3110. DOI: 10.1016/j.jcrysgro.2010.07.059

[17] Gu Y, Zhang YG, Wang K, Fang X, Li C, Zhou L, Li AZ, Li Hsby. Mint: Effects of growth temperature and buffer scheme on characteristics of InP-based metamorphic InGaAs photodetectors. Journal of Grystal Growth. 2013;**378**:65-68. DOI: 10.1016/j.jcrysgro.2012.12.049

[18] Gu Y, Zhang YG, Wang K, Fang X, Li C, Cao YY, Li AZ, Li YY. Mint: InP-based InAs/InGaAs quantum wells with type-I emission beyond 3 μm. Applied Physics Letters. 2011;**99**:081914. DOI: 10.1063/1.3629999

[19] Xi SP, Gu Y, Zhang YG, Chen XY, Zhou L, Li AZ, Li Hsby. Mint: Effects of continuously graded or step-graded $In_xAl_{1-x}As$ buffer on the performance of InP-based $In_{0.83}Ga_{0.17}As$ photodetectors. Journal of Grystal Growth. 2015;**425**:337-340. DOI: 10.1016/j.jcrysgro.2015.03.040

[20] Du B, Gu Y, Zhang YG, Chen XY, Xi SP, Ma YJ, Ji WY, Shi YH. Mint: Effects of continuously or step-continuously graded buffer on the performance of wavelength extended InGaAs photodetectors. Journal of Grystal Growth. 2016;**440**:1-5. DOI: 10.1016/j.jcrysgro.2016.01.016

[21] Jang JH, Cueva G, Hoke WE, Lemonias PJ, Fay P, Adesida I. Mint: Metamorphic graded bandgap InGaAs-InGaAlAs-InAlAs double heterojunction P-i-I-N photodiodes. Journal of Lightwave Technology. 2002;**20**:507-514. DOI: 10.1109/50.989001

[22] Lenox C, Nie H, Kinsey G, Yuan P, Holmes AL, Streetman BG, Campbell JC. Mint: Improved optical response of superlattice graded InAlAs/InGaAs p-i-n photodetectors. Applied Physics Letters. 1998;**73**:3405. DOI: 10.1063/1.122757

[23] Jandl A, Bulsara MT, Fitzgerald EA. Mint: Materials properties and dislocation dynamics in InAsP compositionally graded buffers on InP substrates. Journal of Applied Physics. 2014;**115**:153503. DOI: 10.1063/1.4871289

[24] Zhang YG, Gu Y, Tian ZB, Li AZ, Zhu XR, Wang K. Mint: Wavelength extended InGaAs/InAlAs/InP photodetectors using n-on-p configuration optimized for back illumination. Infrared Physics & Technology. 2009;**52**:52-56. DOI: 10.1016/j.infrared.2008.12.001

[25] Fang X, Gu Y, Chen XY, Zhou L, Cao YY, Li Hsby, Zhang YG. Mint: InP-based $In_xGa_{1-x}As$ metamorphic buffers with different mismatch grading rates. Journal of Semiconductors. 2013;**34**:073005. DOI: 10.1088/1674-4926/34/7/073005

[26] Tersoff J. Mint: Dislocations and strain relief in compositionally graded layers. Applied Physics Letters. 1993;**62**:693. DOI: 10.1063/1.108842

[27] Boschetti A, Bassi D, Iacob E, Iannotta S, Ricci L, Scotoni M. Mint: Resonant photoacoustic simultaneous detection of methane and ethylene by means of a 1.63 μm diode laser. Applied Physics B-Lasers and Optics. 2002;**74**:273-278. DOI: 10.1007/s003400200790

[28] Fang X, Gu Y, Zhang YG, Zhou L, Zhou L, Wang K, Li Hsby, Liu KH, Cao YY. Mint: Effects of compositional overshoot on InP-based InAlAs metamorphic graded buffer. Journal of Infrared Millimeter Waves. 2013;**32**:481-490. DOI: 10.3724/SP.J.1010.2013.00481

[29] Gu Y, Zhang YG, Wang K, Fang X, Liu KH. Mint: InAlAs graded metamorphic buffer with digital alloy intermediate layers. Japanese Journal of Applied Physics. 2012;**51**:080205. DOI: 10.1143/JJAP.51.080205

[30] Chen XY, Zhang YG, Gu Y, Zhou L, Cao YY, Fang X, Li Hsby. Mint: GaAs-based $In_{0.83}Ga_{0.17}As$ photodetector structure grown by gas source molecular beam epitaxy. Journal of Grystal Growth. 2014;**39**:75-80. DOI: 10.1016/j.jcrysgro.2013.11.083

[31] Zhang YG, Gu Y, Wang K, Li AZ, Li C. Mint: Properties of gas source molecular beam epitaxy grown wavelength extended InGaAs photodetector structures on a linear graded InAlAs buffer. Semiconductor Science and Technology. 2008;**23**:125029. DOI: 10.1088/0268-1242/23/12/125029

[32] Zhou L, Zhang YG, Chen XY, Gu Y, Li Hsby, Cao YY, Xi SP. Mint: Dark current characteristics of GaAs-based 2.6 μm InGaAs photodetectors on different types of InAlAs buffer layers. Journal of Physics D: Applied Physics. 2014;**47**:085107. DOI: 10.1088/0022-3727/47/8/085107

[33] Guillot G, Bremond G, Benyattou T, Ducroquet F, Wirth B, Colombet M, Louati A, Bencherifa A. Mint: Identification of the Fe acceptor level in $Ga_{0.47}In_{0.53}As$. Semiconductor Science Technology. 1990;**5**:391-394. DOI: 10.1088/0268-1242/5/5/003

[34] Pal C, Gombia E, Mosca R, Bosacchi A, Franchi S. Mint: Deep levels in virtually unstrained InGaAs layers deposited on GaAs. Journal of Applied Physics. 1998;**84**:2965-2967. DOI: 10.1063/1.368404

[35] Ji XL, Liu BQ, Tang HJ, Yang XL, Li X, Gong HM, Shen B, Han P, Yan F. Mint: 2.6 μm MBE grown InGaAs detectors with dark current of SRH and TAT. AIP Advances. 2014;**4**:087135. DOI: 10.1063/1.4894142

[36] Henager CH, Hoagland RG. Mint: A rebound mechanism for misfit dislocation creation in metallic nanolayers. Scripta Materialia. 2004;**50**:701-705. DOI: 10.1016/j.scriptamat.2003.09.002

[37] Wang Y, Ruterana P, Desplanque L, ElKazzi S, Wallart X. Mint: Growth mode dependence of misfit dislocation configuration at lattice mismatched III-V semiconductor interfaces. Europhysics Letters. 2012;**97**:68011. DOI: 10.1209/0295-5075/97/68011

[38] Chen XY, Gu Y, Zhang YG, Xi SP, Guo ZX, Zhou L, Li AZ, Li Hsby. Mint: Optimization of InAlAs buffers for growth of GaAs-based high indium content InGaAs photodetectors. Journal of Grystal Growth. 2015;**425**:346-350. DOI: 10.1016/j.jcrysgro.2015.02.102

[39] Samavedan SB, Fitzgerald EA. Mint: Novel dislocation structure and surface morphology effects in relaxed Ge/Si-Ge(graded)/Si structures. Journal of Applied Physics. 1997;**81**:3108. DOI: 10.1063/1.364345

[40] Tersoff J. Mint: Stress-induced roughening in epitaxial growth. Applied Surface Science. 1996;**102**:1-2. DOI: 10.1016/0169-4332(96)00002-5

[41] France RM, Geisz JF, Steiner MA, To B, Romero MJ, Olavarria WJ, King RR. Mint: Reduction of crosshatch roughness and threading dislocation density in metamorphic GaInP buffers and GaInAs solar cells. Journal of Applied Physics. 2012;**111**:103528. DOI: 10.1063/1.4721367

[42] Ayers JE. Mint: The measurement of threading dislocation densities in semiconductor crystals by X-ray diffraction. Journal Crystal Growth. 1994;**135**:71-77. DOI: 10.1016/0022-0248(94)90727-7

[43] Andrews AM, Speck JS, Romanov AE, Bobeth M, Pompe W. Mint: Modeling cross-hatch surface morphology in growing mismatched layers. Journal of Applied Physics. 2002; **91**:1933. DOI: 10.1063/1.1428091

[44] Cullis AG, Pidduck AJ, Emeny MT. Mint: Misfit dislocation sources at surface ripple troughs in continuous heteroepitaxial layers. Physical Review Letters. 1995;**75**:2368-2371. DOI: 10.1103/PhysRevLett.75.2368